Electronic Supplementary Material (ESI) for Journal of Materials Chemistry A.
This journal is © The Royal Society of Chemistry 2021

Supporting Information

Melt-Quenched Porous Organic Cage Glasses

Michael C. Brand,[a] Francesca Greenwell,[a] Rob Clowes,[a] Benjamin D. Egleston,[a] Aiting Kai,[a] Andrew I. Cooper,[a*] Thomas D. Bennett,[b*] Rebecca L. Greenaway[a,c*]

[a] Department of Chemistry and Materials Innovation Factory, University of Liverpool, 51 Oxford Street, Liverpool, L7 3NY, UK;

[b] Department of Materials Science and Metallurgy, University of Cambridge, 27 Charles Babbage Road, Cambridge CB3 0FS, UK;

[c] Department of Chemistry, Molecular Sciences Research Hub, Imperial College London, White City Campus, 82 Wood Lane, W12 0BZ, UK.

Emails: aicooper@liverpool.ac.uk, tdb35@cam.ac.uk, r.greenaway@imperial.ac.uk

Supplementary Figures

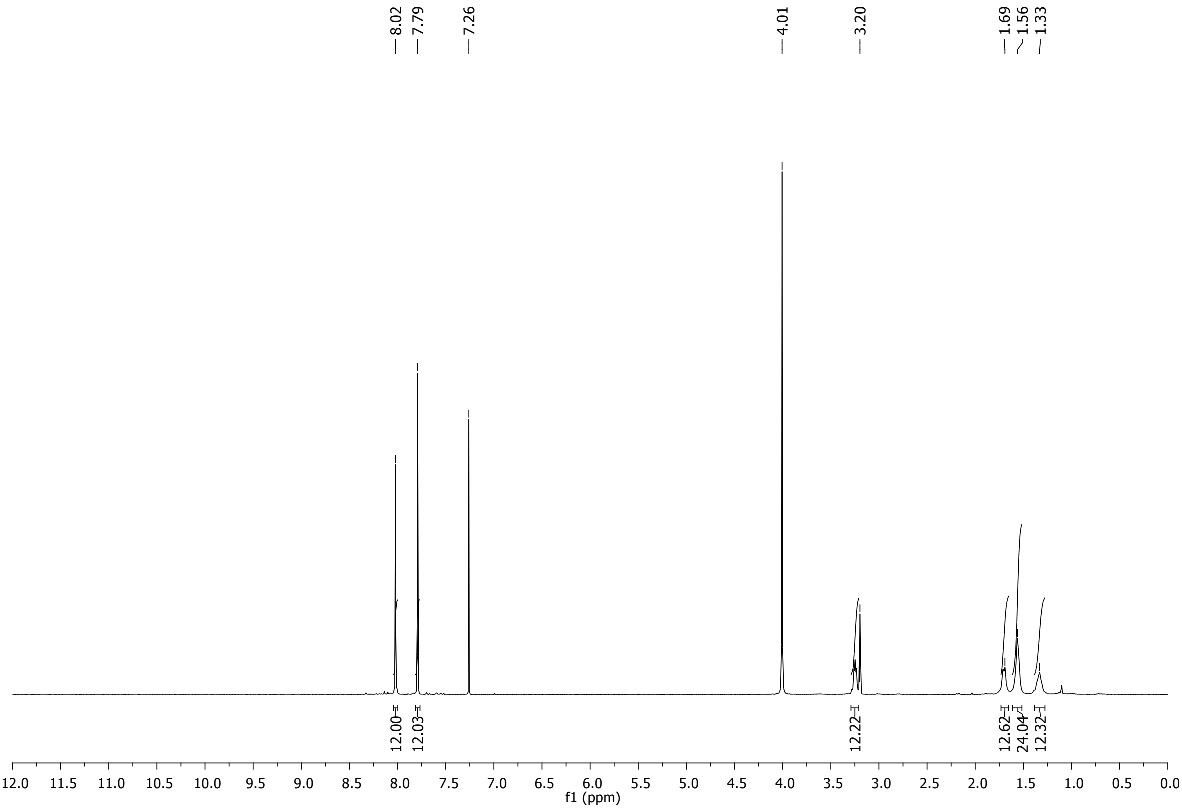

Supplementary Figure 1: ^{1}H NMR ($CDCl_3$:d_4-MeOD) spectra of **CC3**-*S*

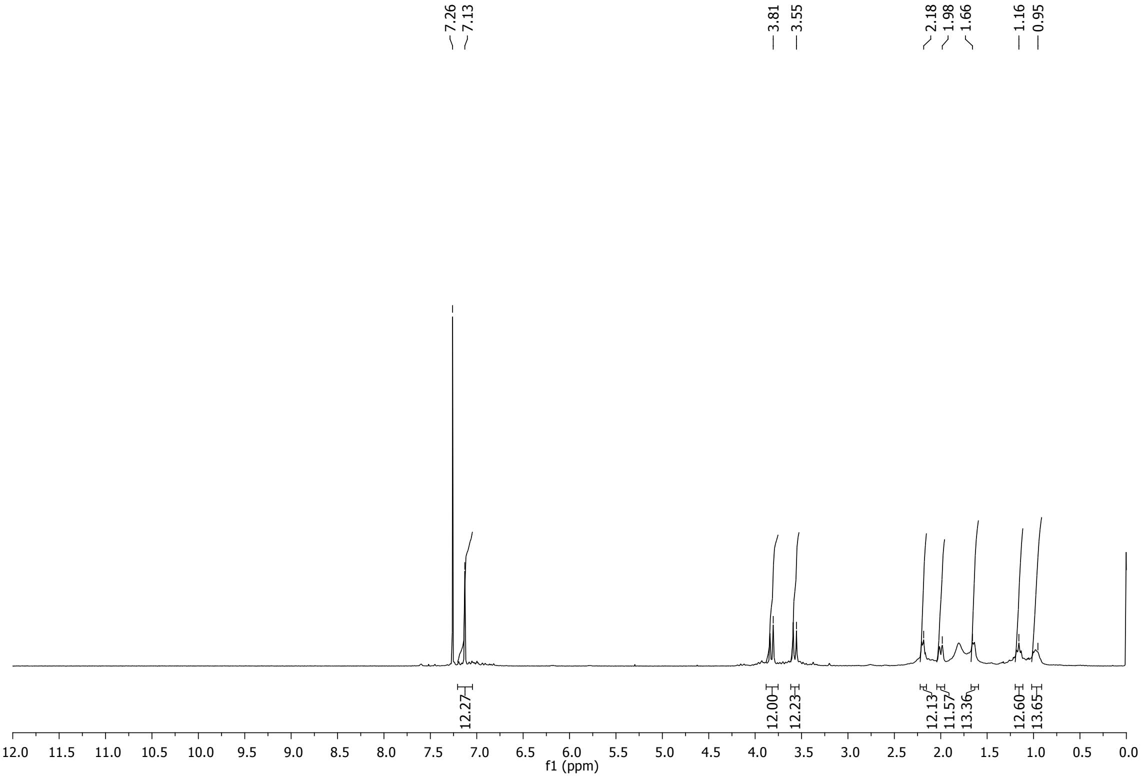

Supplementary Figure 2: ^{1}H NMR ($CDCl_3$) spectra of **RCC3**-*S*

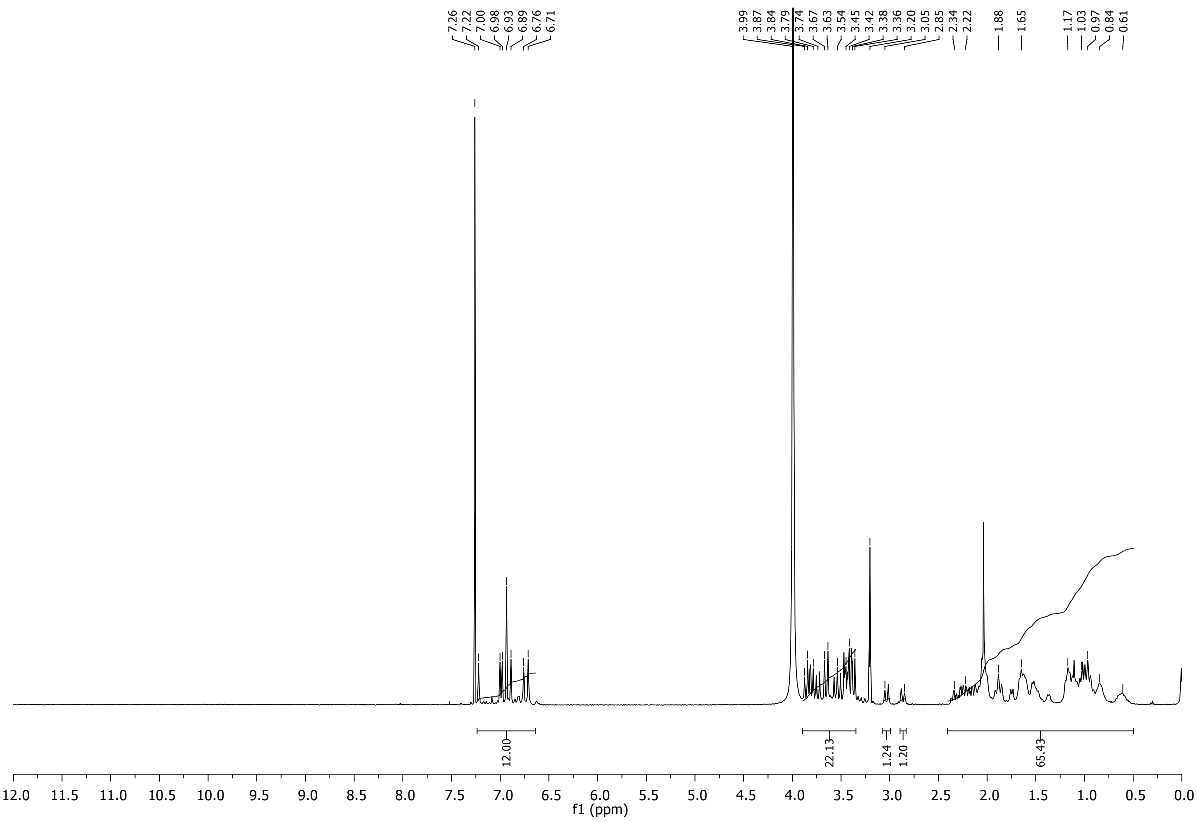

Supplementary Figure 3: ^{1}H NMR ($CDCl_3$:d_4-MeOD) spectra of **AT-RCC3**-*S*

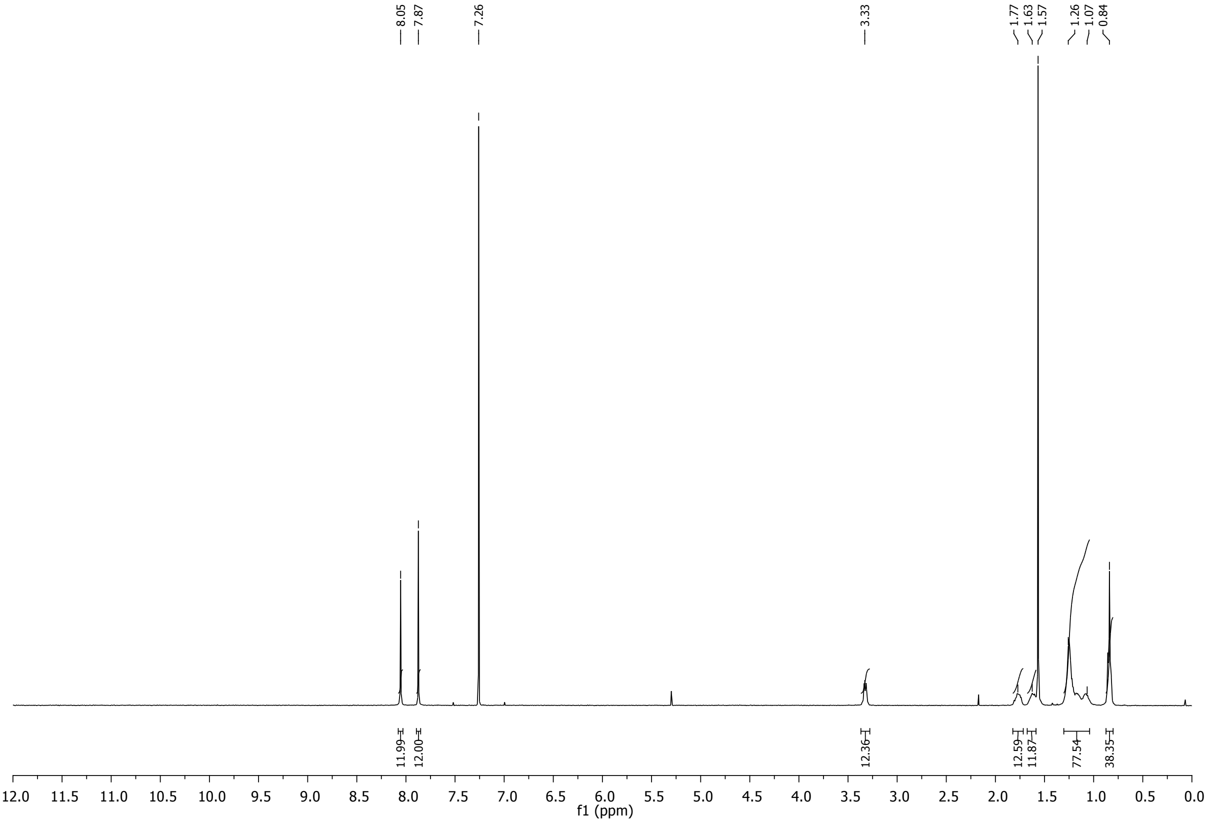

Supplementary Figure 4: ^{1}H NMR ($CDCl_3$) spectra of ***n*C$_5$-CC** (pentyl cage)

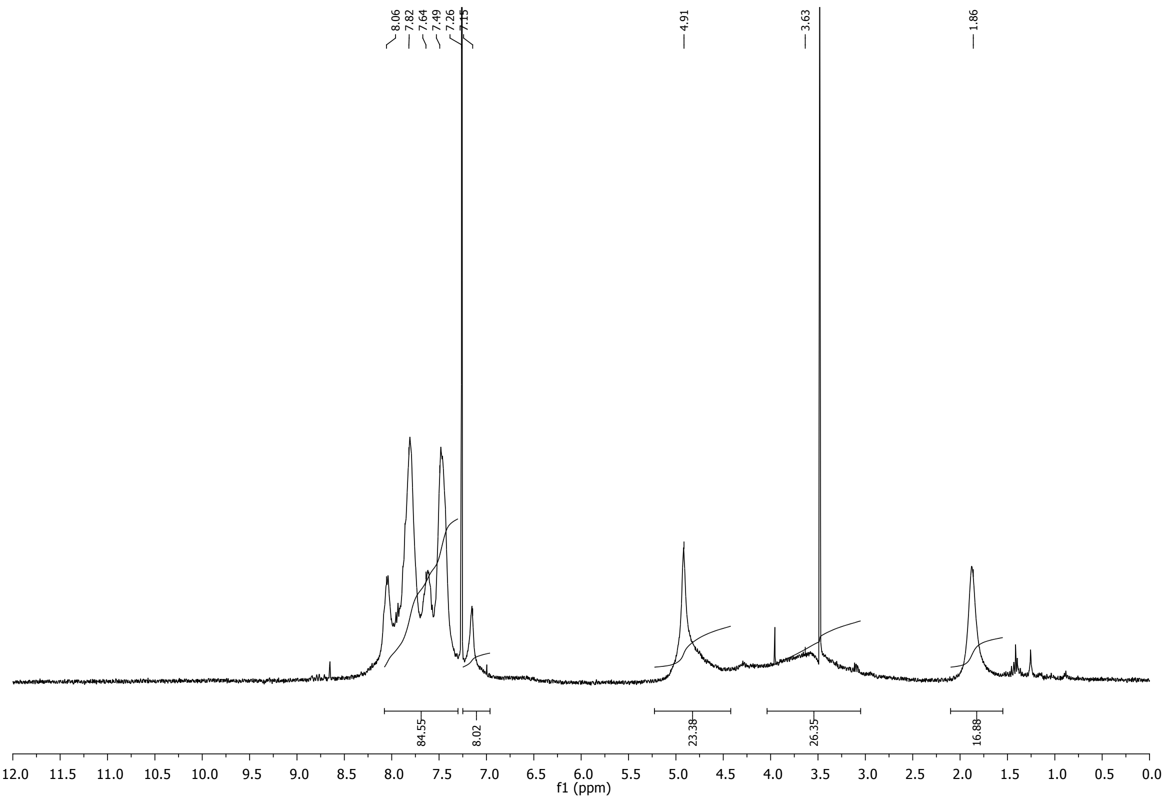

Supplementary Figure 5: ^{1}H NMR ($CDCl_3$) spectra of **RCC1b**

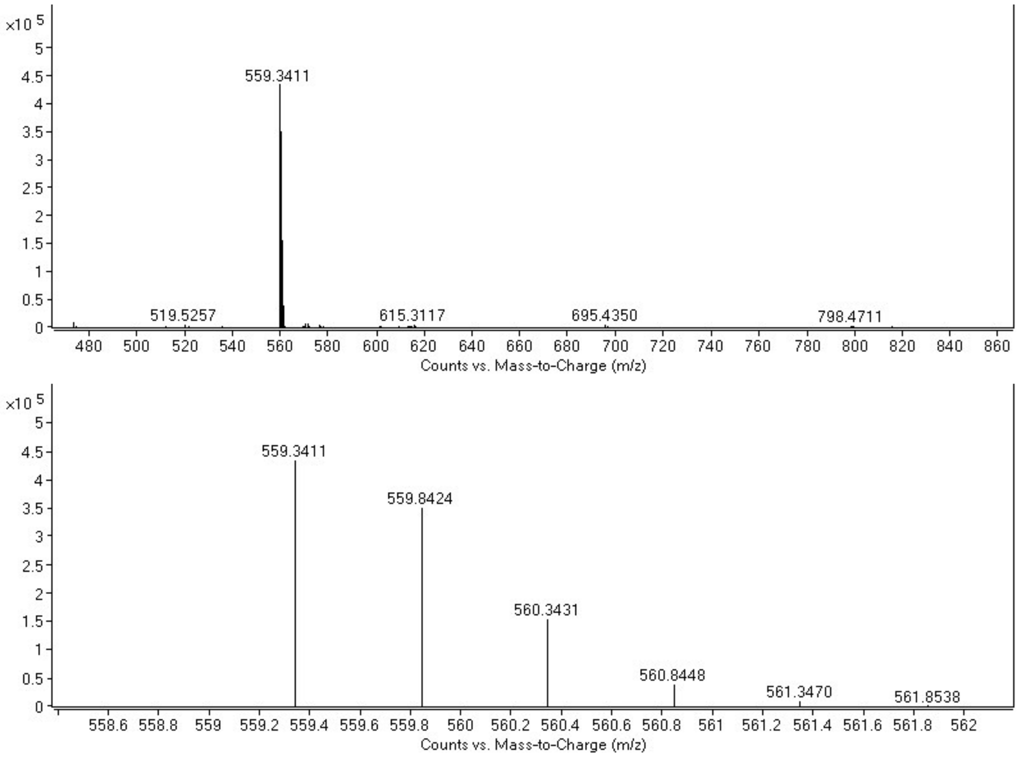

Supplementary Figure 6: HRMS spectra of **CC3**-*S*

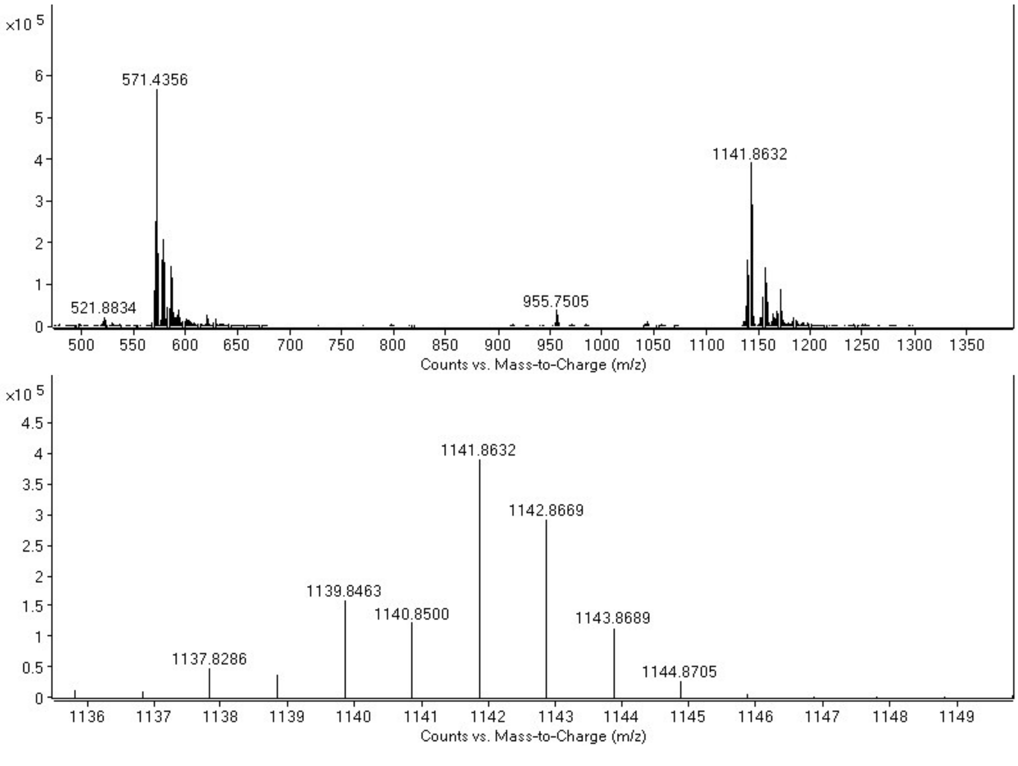

Supplementary Figure 7: HRMS spectra of **RCC3**-*S*

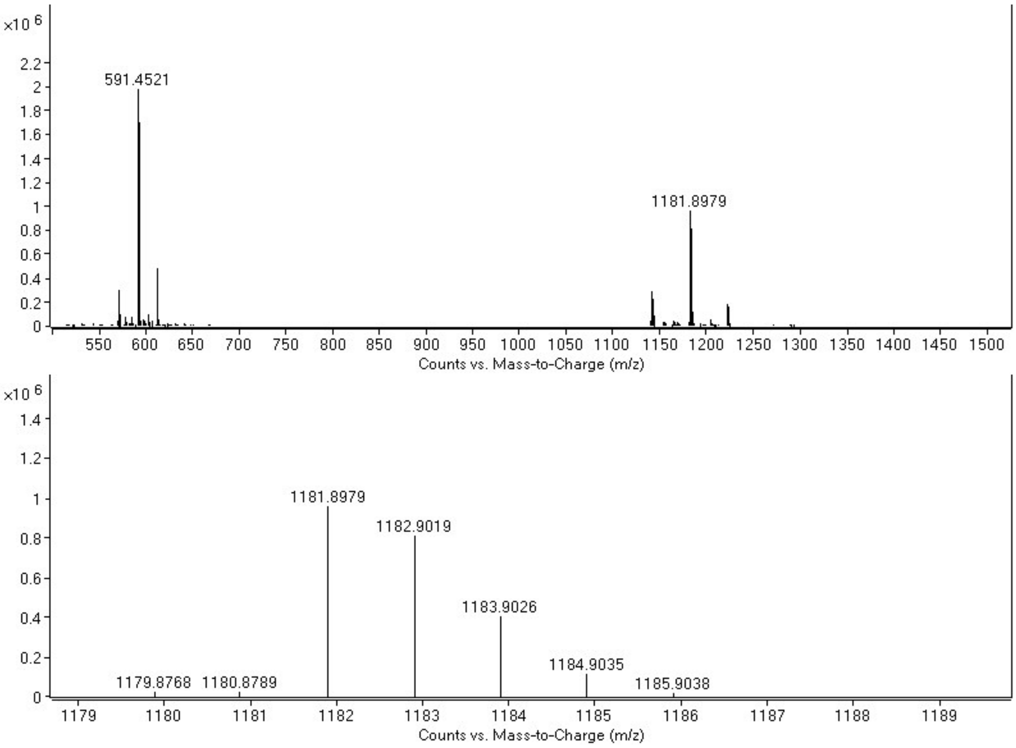

Supplementary Figure 8: HRMS spectra of **AT-RCC3**-*S*

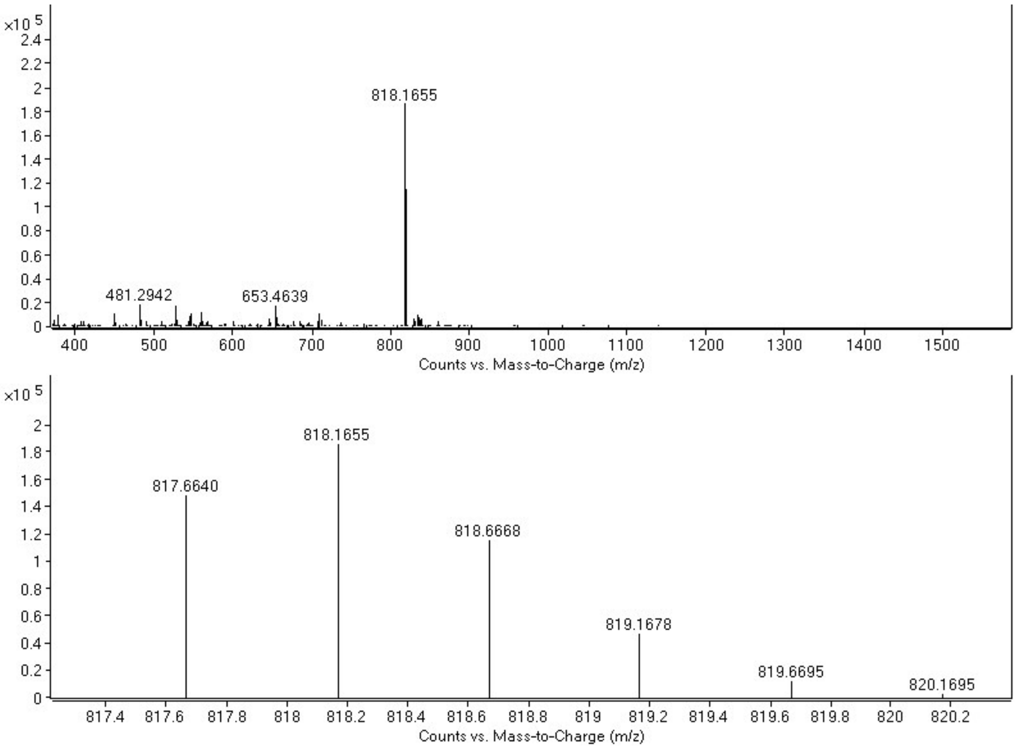

Supplementary Figure 9: HRMS spectra of ***n*C_5-CC** (pentyl cage)

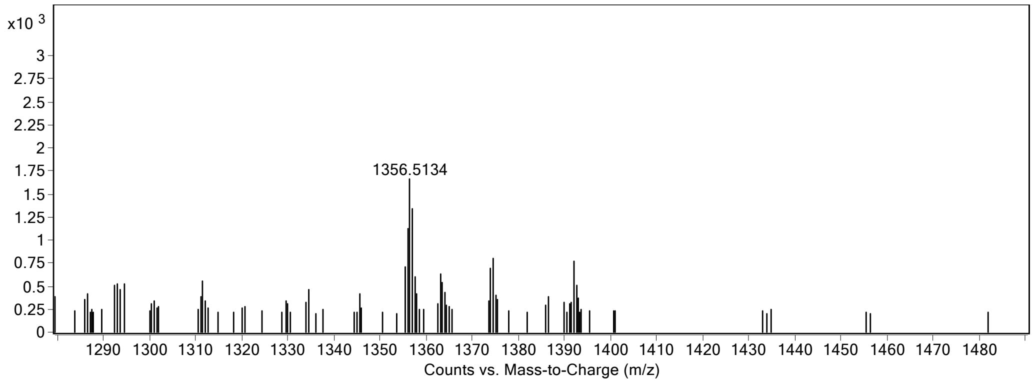

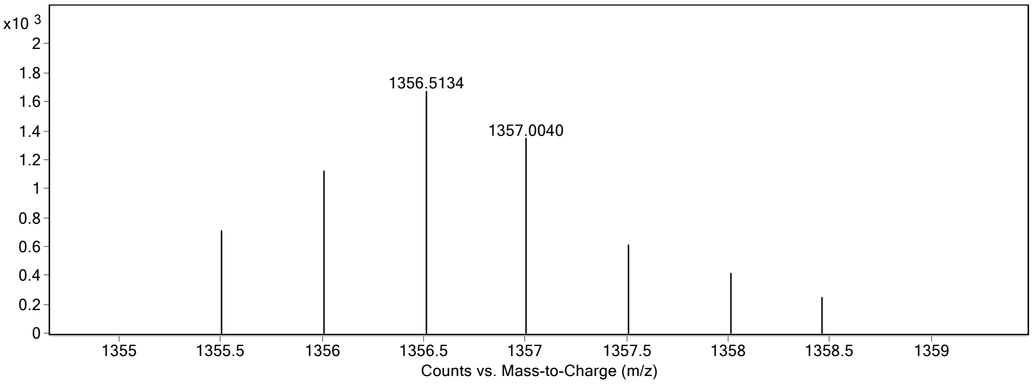

Supplementary Figure 10: HRMS spectra of **RCC1b**

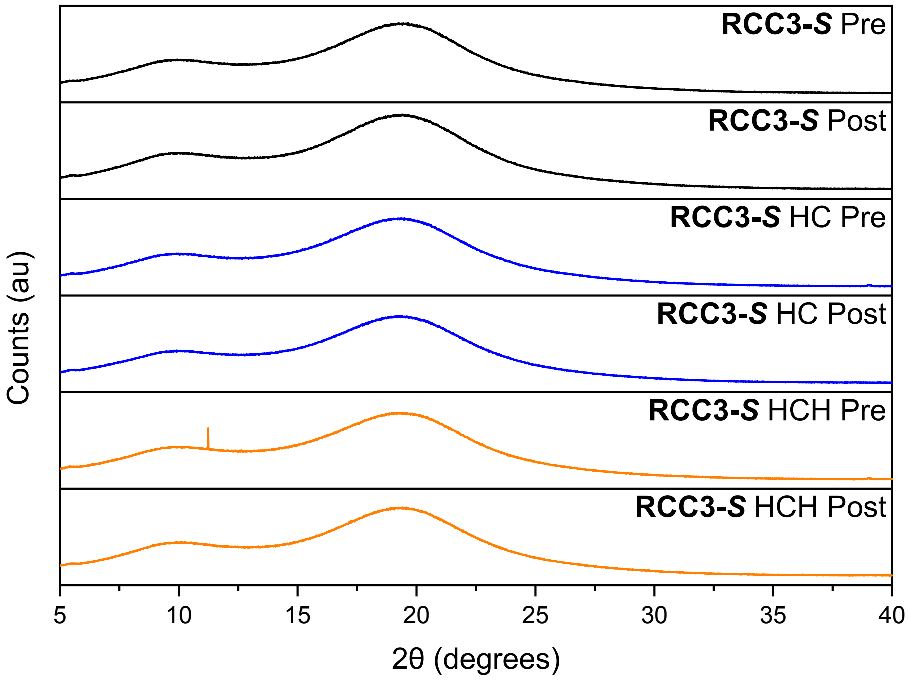

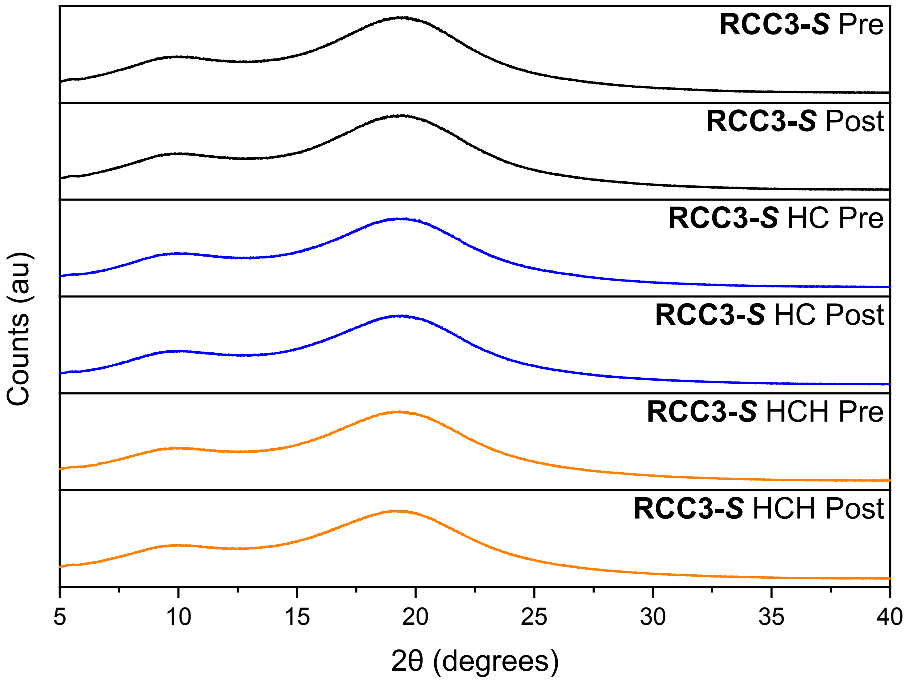

Supplementary Figure 11: Stacked PXRDs of desolvated **RCC3**-*S* samples pre- and post-sorption, prior to heating (black), after a heat-cool (HC) cycle (blue), and after a heat-cool-heat (HCH) cycle (orange), to 250 °C (top) and 300 °C (bottom).

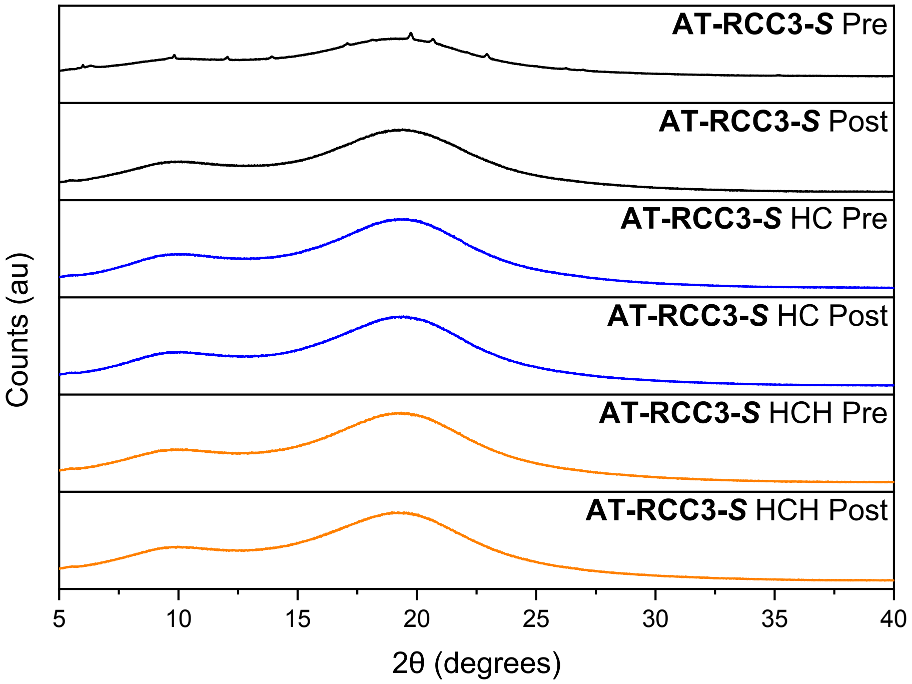

Supplementary Figure 12: Stacked PXRDs of desolvated **AT-RCC3**-*S* samples pre- and post-sorption, prior to heating (upper, black), after a heat-cool (HC) cycle to 250 °C (middle, blue), and after a heat-cool-heat (HCH) cycle to 250 °C (lower, orange).

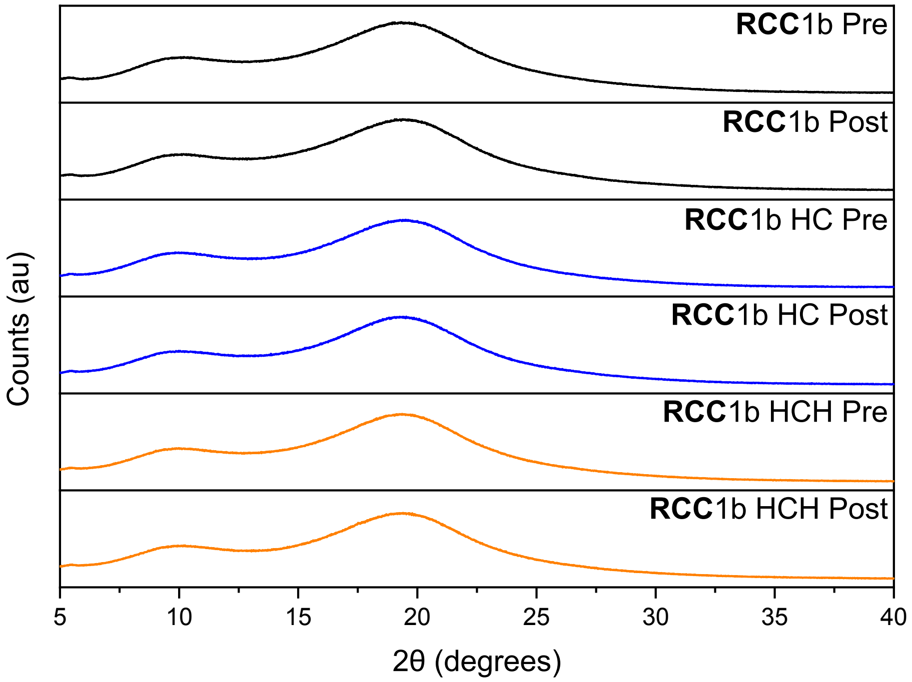

Supplementary Figure 13: Stacked PXRDs of desolvated **RCC1b** samples pre- and post-sorption, prior to heating (upper, black), after a heat-cool (HC) cycle to 280 °C (middle, blue), and after a heat-cool-heat (HCH) cycle to 280 °C (lower, orange).

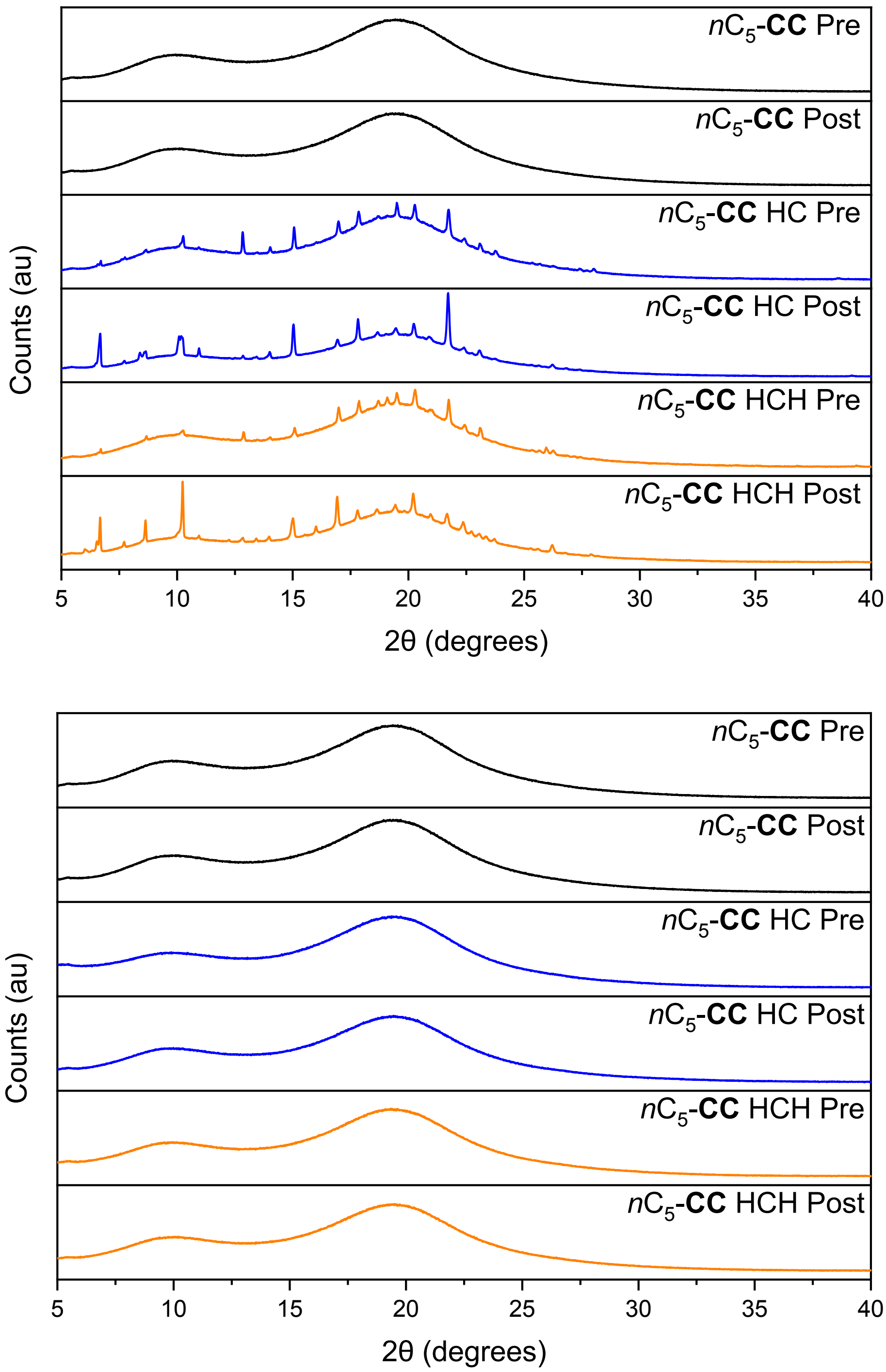

Supplementary Figure 14: Stacked PXRDs of desolvated ***n*C$_5$-CC** (pentyl cage) samples pre- and post-sorption, prior to heating (black), after a heat-cool (HC) cycle (blue), and after a heat-cool-heat (HCH) cycle (orange), to 170 °C (top) and 260 °C (bottom).

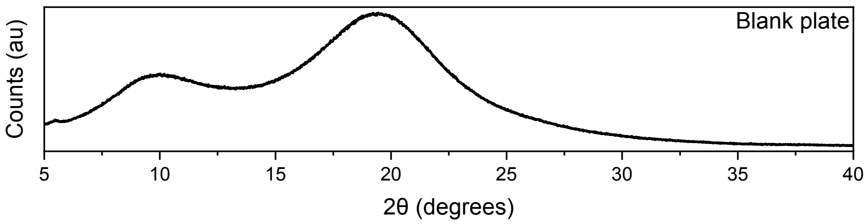

Supplementary Figure 15: PXRD pattern of a blank sample in an empty well of the 96-well ProxiPlate

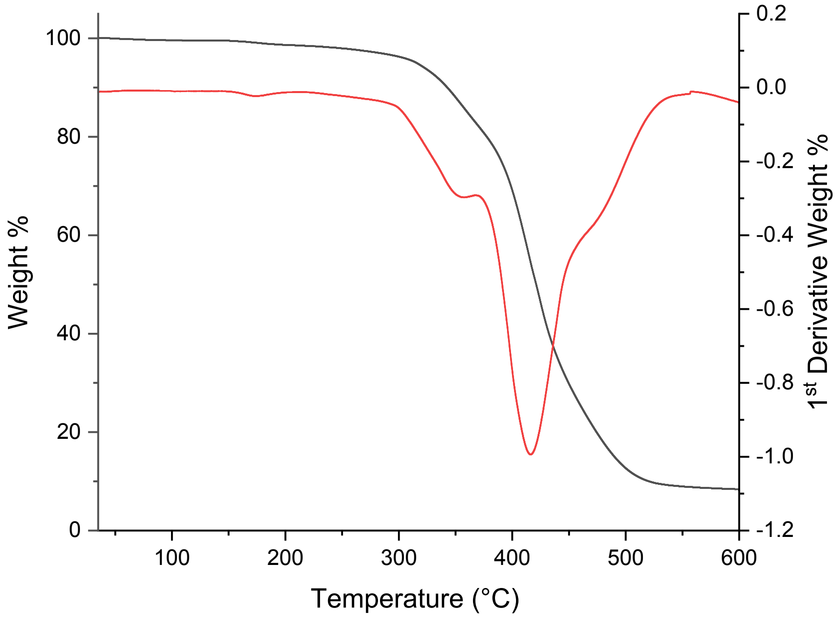

Supplementary Figure 16: TGA trace of **RCC3**-*S*, desolvated in a vacuum oven at 130 °C until no significant mass loss was observed.

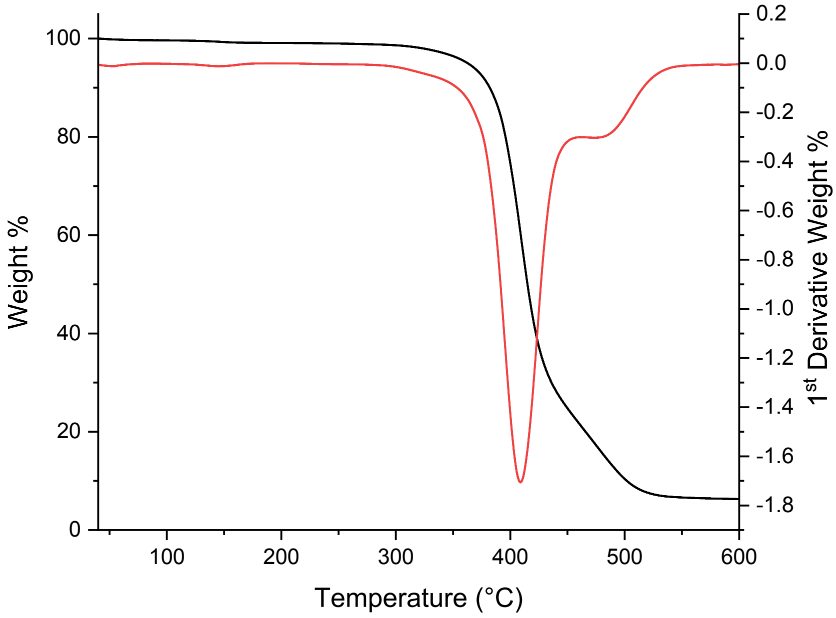

Supplementary Figure 17: TGA trace of **AT**-**RCC3**-*S*, desolvated in a vacuum oven at 90 °C until no significant mass loss was observed.

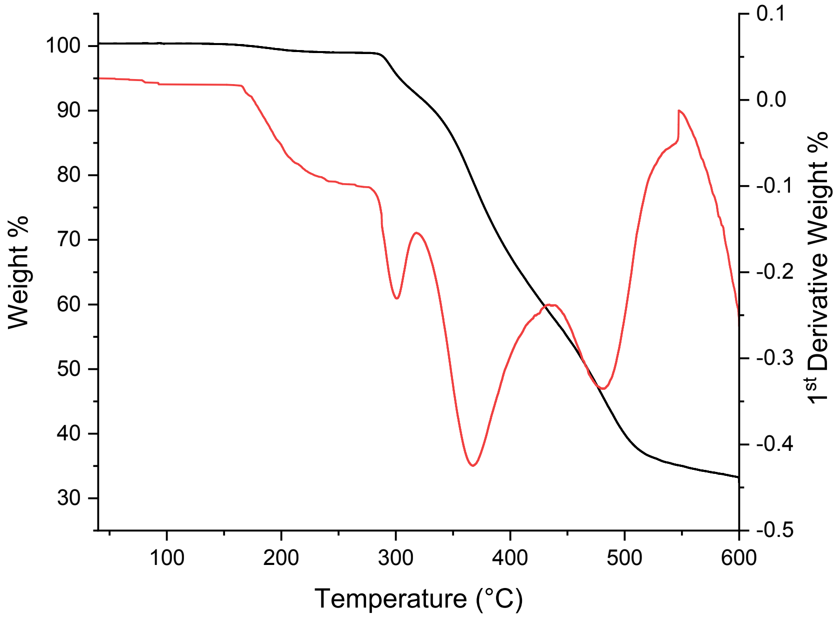

Supplementary Figure 18: TGA trace of ***n*C$_5$-CC** (pentyl cage), desolvated in a vacuum oven at 90 °C until no significant mass loss was observed.

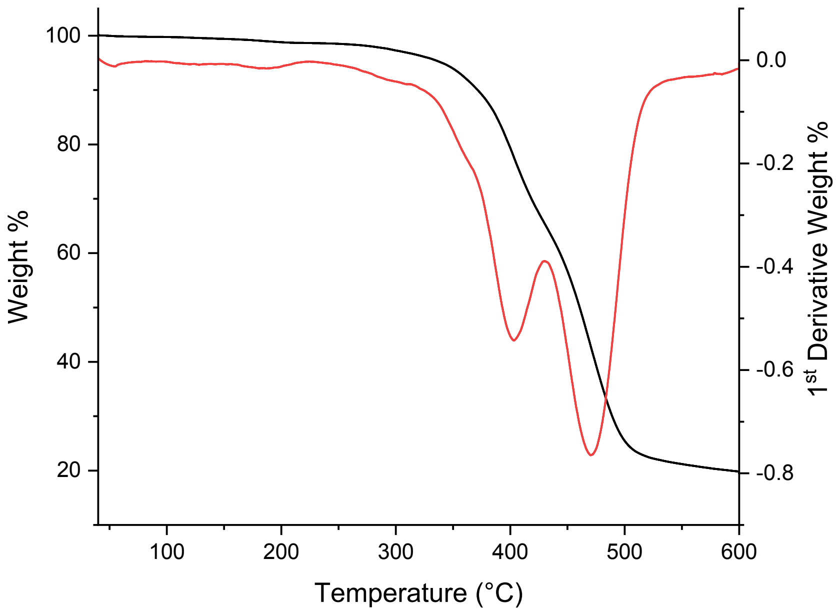

Supplementary Figure 19: TGA trace of **RCC1b**, desolvated in a vacuum oven at 90 °C until no significant mass loss was observed.

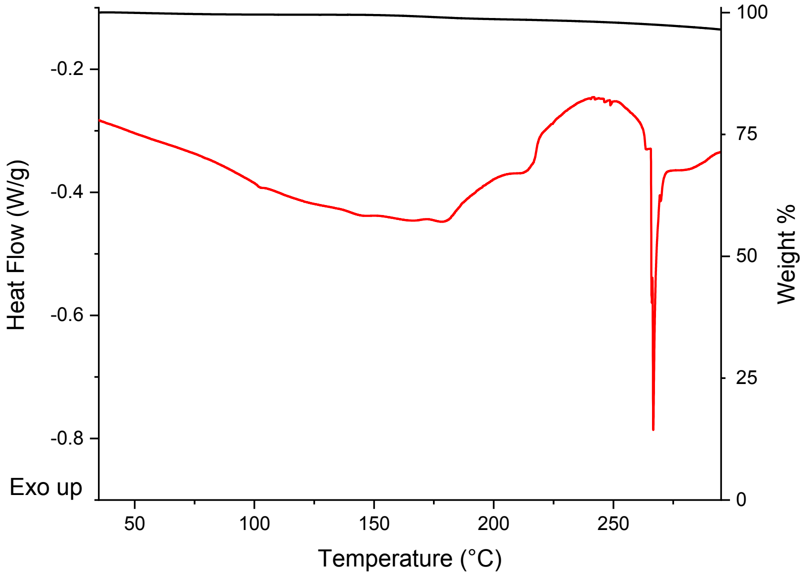

Supplementary Figure 20: Initial DSC trace (red) of desolvated **RCC3**-*S* heated to 300 °C, with corresponding TGA curve (black).

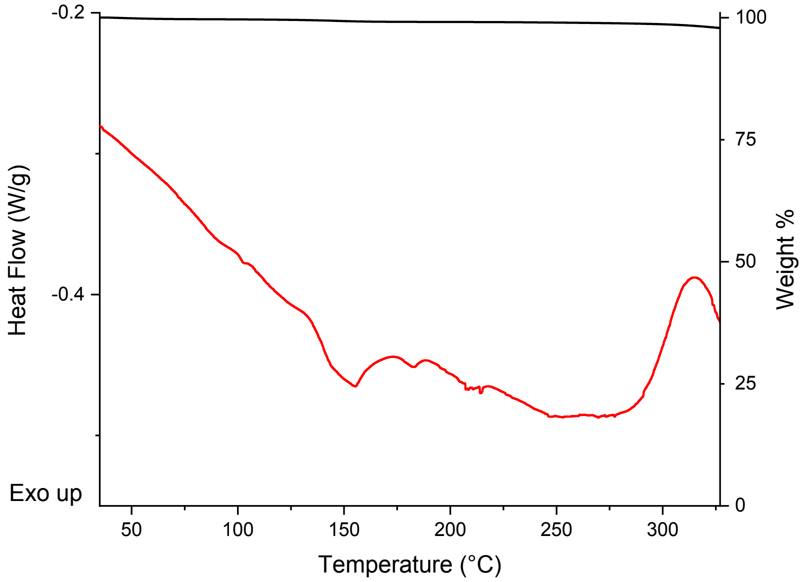

Supplementary Figure 21: Initial DSC trace (red) of desolvated **AT-RCC3**-*S* heated to 330 °C, with corresponding TGA curve (black).

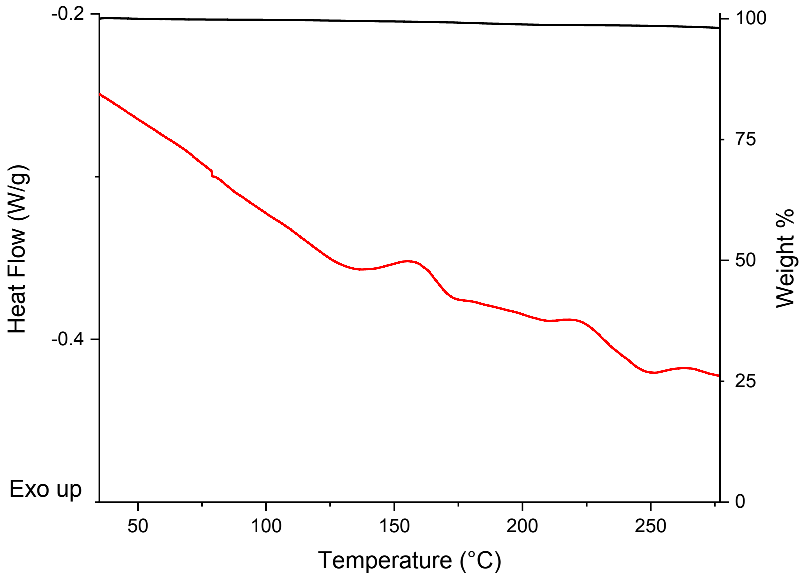

Supplementary Figure 22: Initial DSC trace (red) of desolvated **RCC1b** heated to 280 °C, with corresponding TGA curve (black).

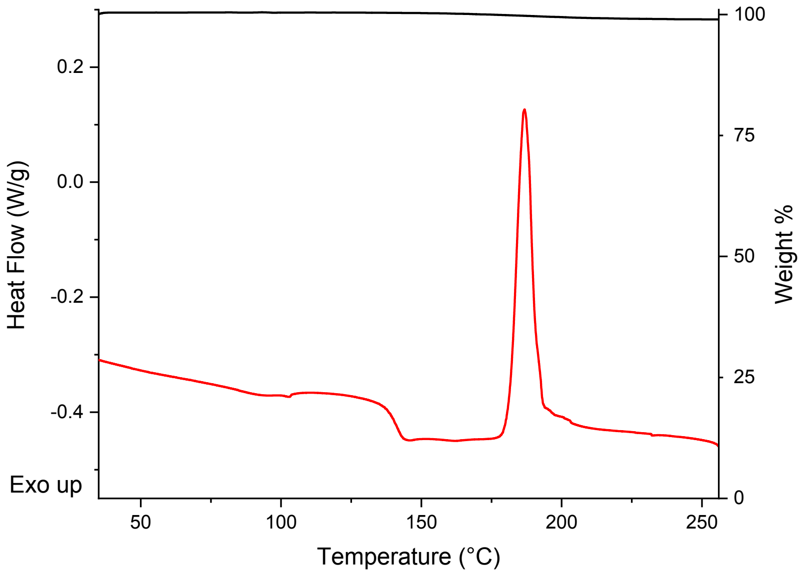

Supplementary Figure 23: Initial DSC trace (red) of desolvated ***n*$\mathbf{C_5}$-CC** heated to 260 °C, with corresponding TGA curve (black).

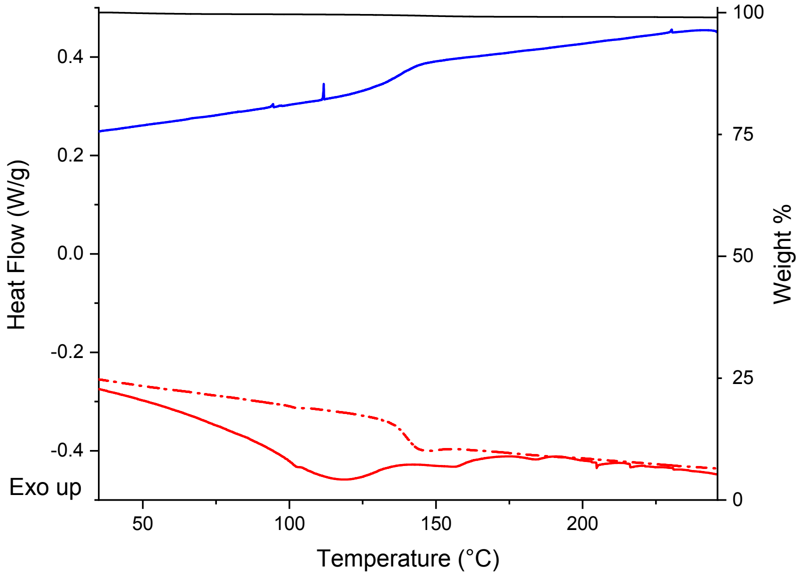

Supplementary Figure 24: DSC trace of desolvated **AT-RCC3**-*S* sample subjected to heat-cool-heat (HCH) cycle to 250 °C, with corresponding TGA curve (black). DSC trace: initial upscan shown as a solid red line, downscan as a blue line, and second upscan as a dashed red line.

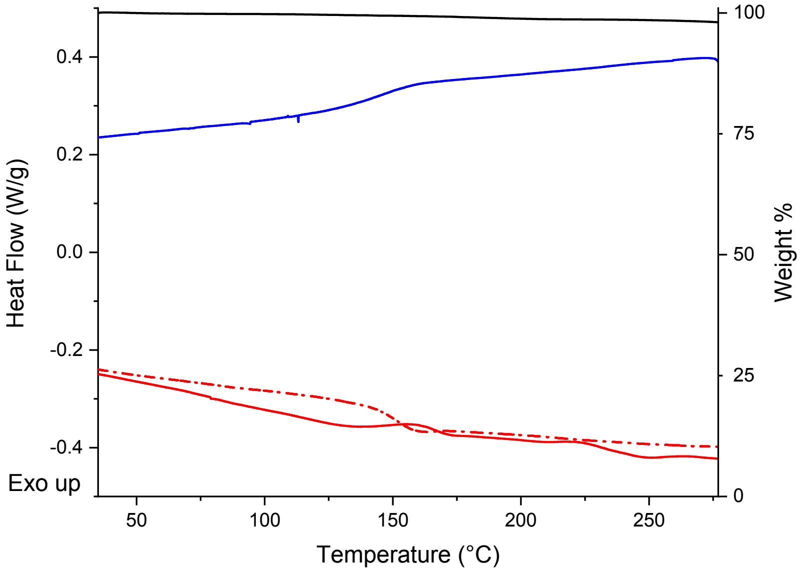

Supplementary Figure 25: DSC traces of desolvated **RCC1b** samples subjected to heat-cool-heat (HCH) cycle to 280 °C, with corresponding TGA curve (black). DSC trace: initial upscan shown as a solid red line, downscan as a blue line, and second upscan as a dashed red line.

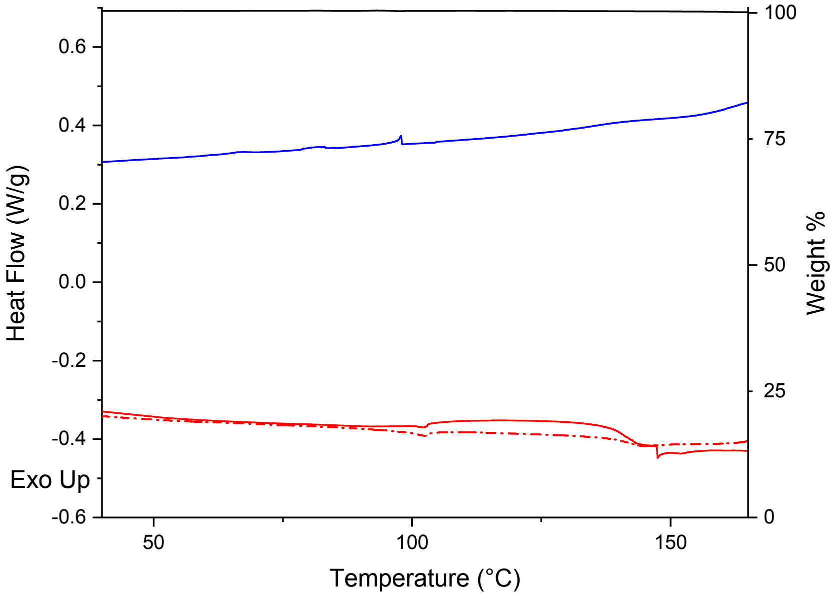

Supplementary Figure 26: DSC traces of desolvated ***n*C$_5$-CC** (pentyl cage) samples subjected to heat-cool-heat (HCH) cycle to 170 °C, with corresponding TGA curve (black). DSC trace: initial upscan shown as a solid red line, downscan as a blue line, and second upscan as a dashed red line.

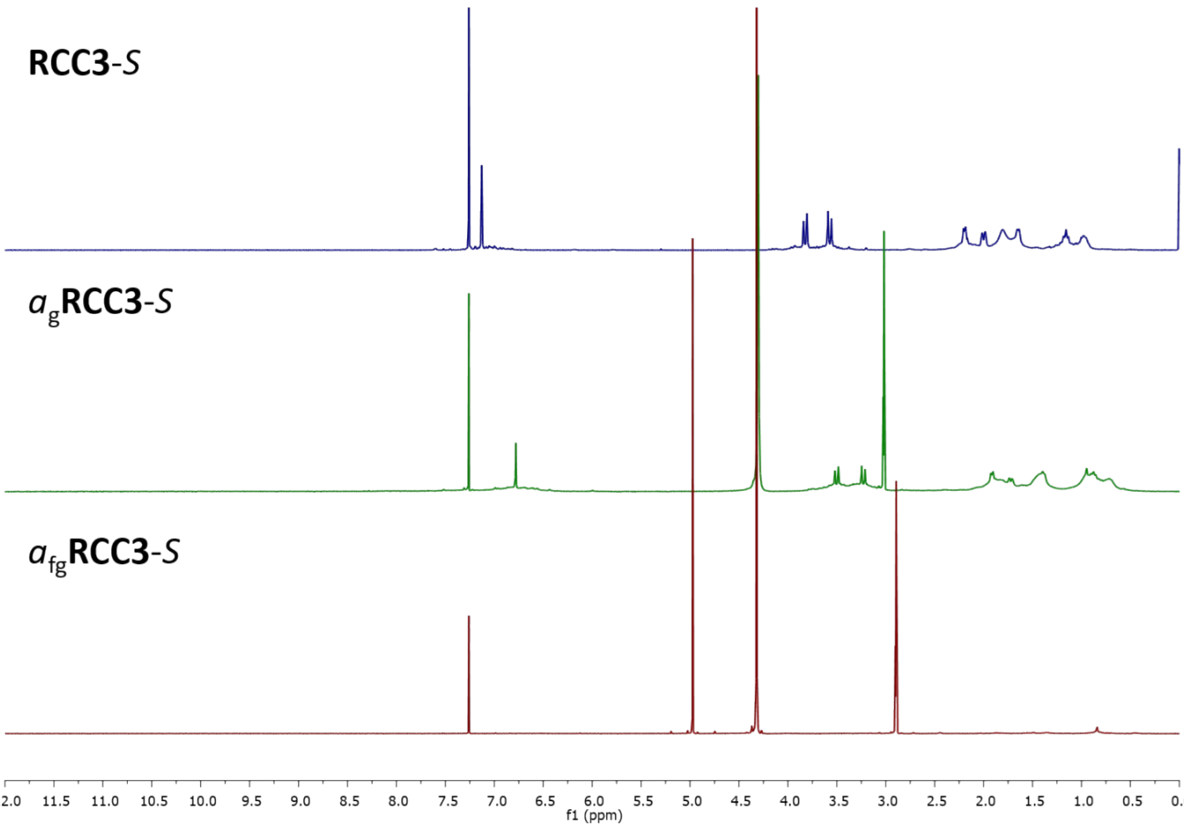

Supplementary Figure 27: Stacked ^{1}H NMR spectra of **RCC3**-*S* ($CDCl_3$), a_g**RCC3**-*S* ($CDCl_3$:d_4-MeOD), and a_{fg}**RCC3**-*S* ($CDCl_3$:d_4-MeOD).

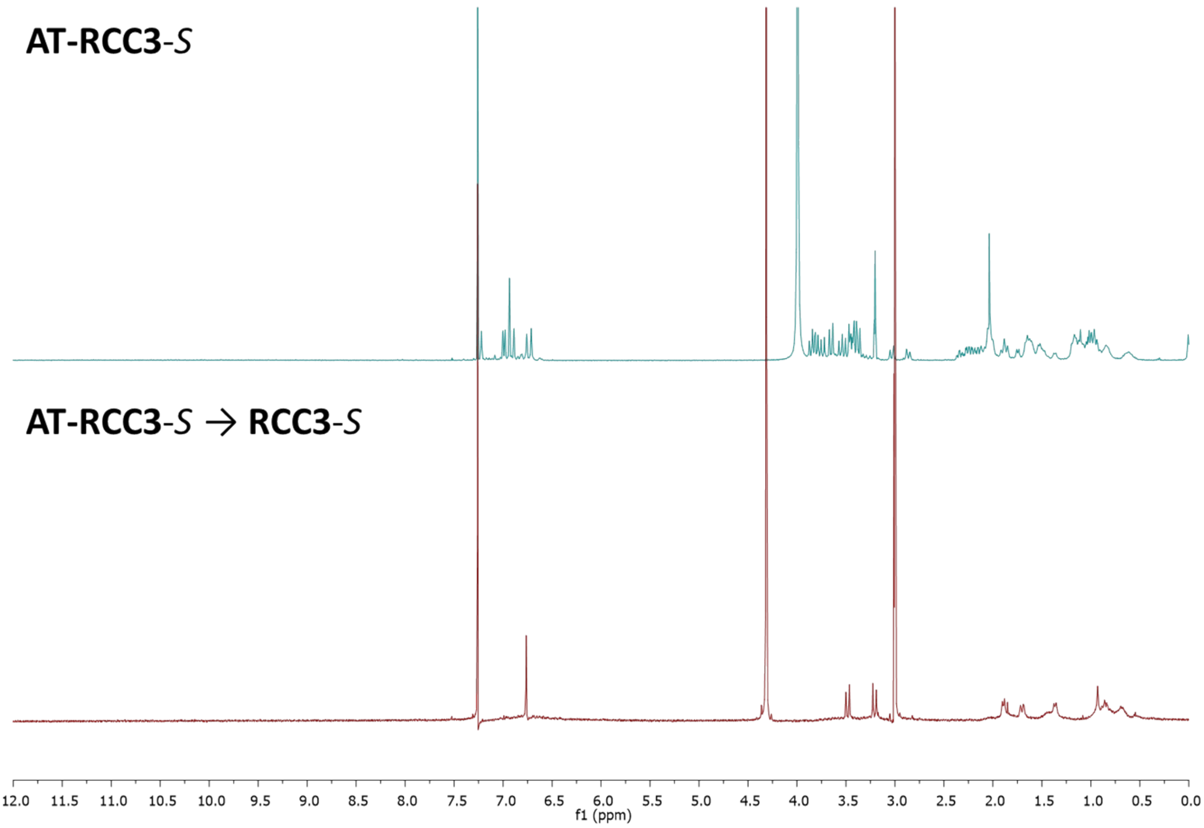

Supplementary Figure 28: Stacked ^{1}H NMR spectra of **AT-RCC3**-*S* ($CDCl_3$:d_4-MeOD) and the glass formed from heating and cooling **AT-RCC3**-*S* ($CDCl_3$:d_4-MeOD).

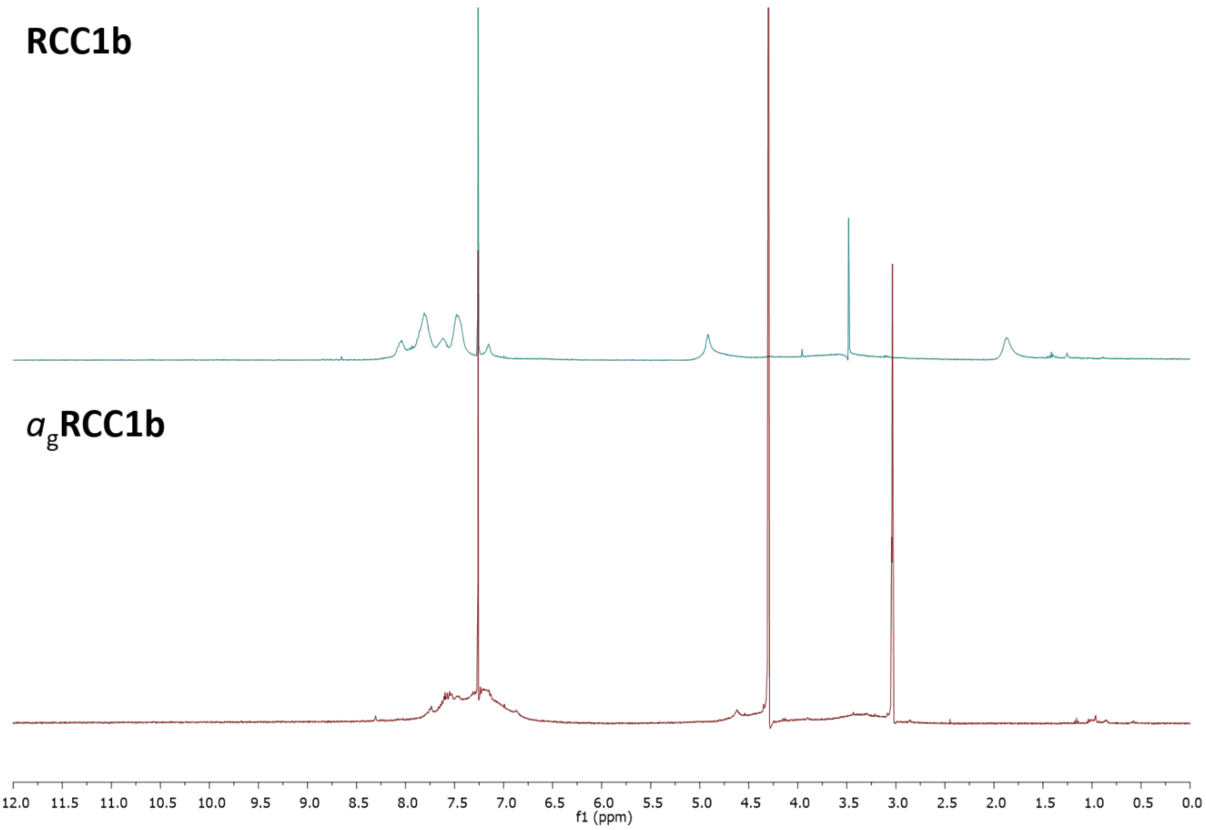

Supplementary Figure 29: Stacked ^{1}H NMR spectra of **RCC1b** ($CDCl_3$) and a_g**RCC1b** ($CDCl_3$:d_4-MeOD).

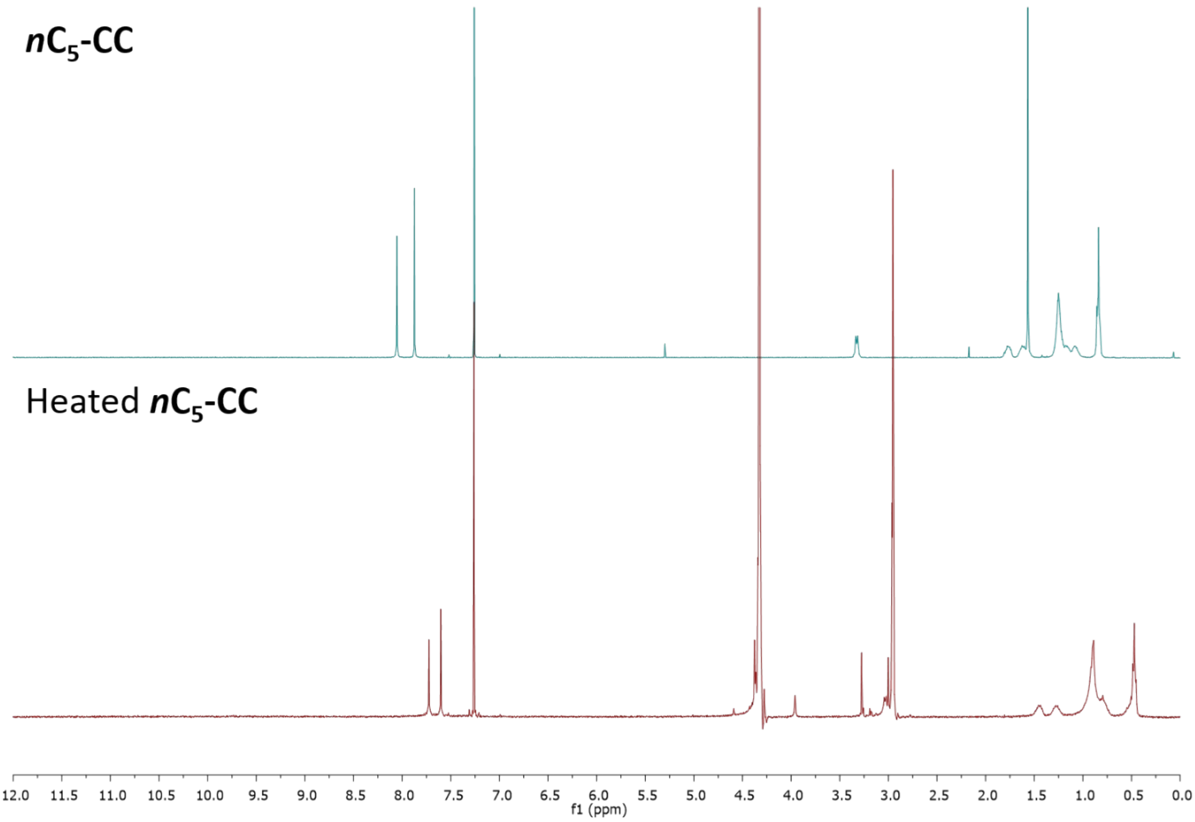

Supplementary Figure 30: Stacked ^{1}H NMR spectra of ***n*C$_5$-CC** before ($CDCl_3$), and after ($CDCl_3$:d$_4$-MeOD), a heat-melt-cool cycle to 170 °C.

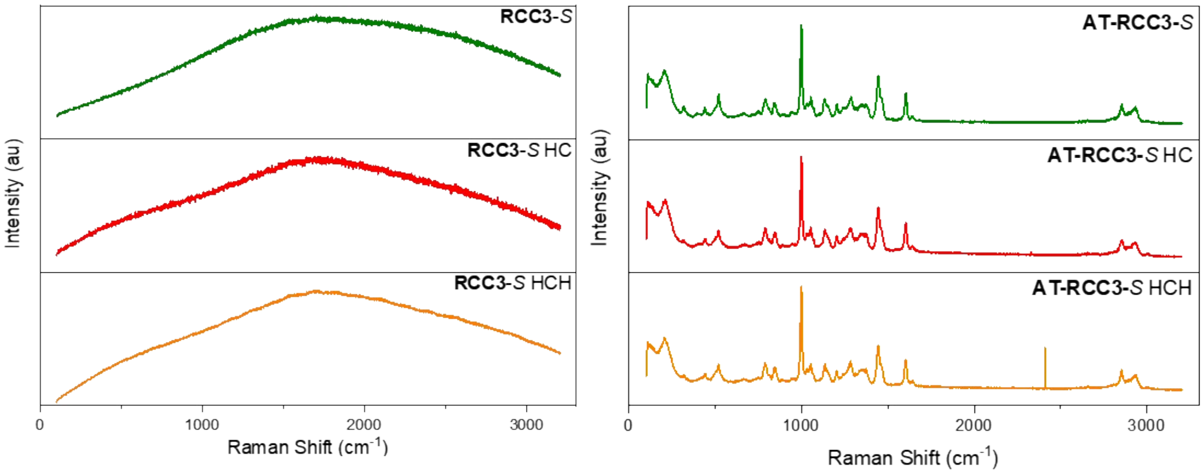

Supplementary Figure 31: Stacked Raman spectra of **RCC3**-*S* and **AT-RCC3**-*S* with their respective glasses. Green - material as prepared; Red - material after a heat-cool (HC) cycle; orange - material after heat-cool-heat (HCH) cycle.

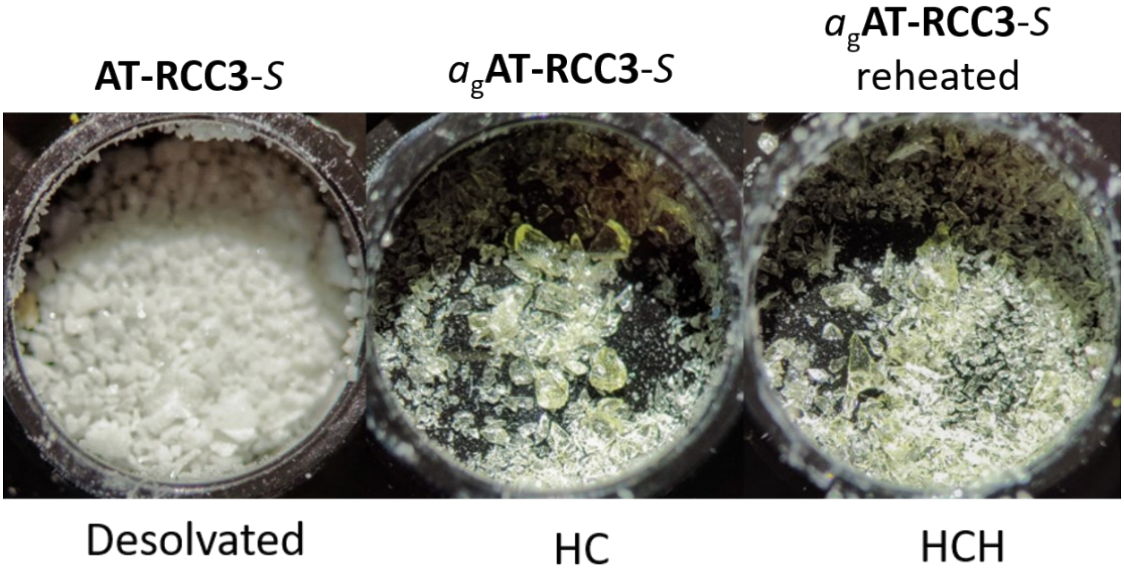

Supplementary Figure 32: Optical images of desolvated **AT-RCC3**-*S* sample prior to heating (left), a_g**AT-RCC3**-*S* after a heat-cool (HC) cycle to 250 °C (middle), and reheated a_g**AT-RCC3**-*S* after a heat-cool-heat (HCH) cycle to 250 °C (right).

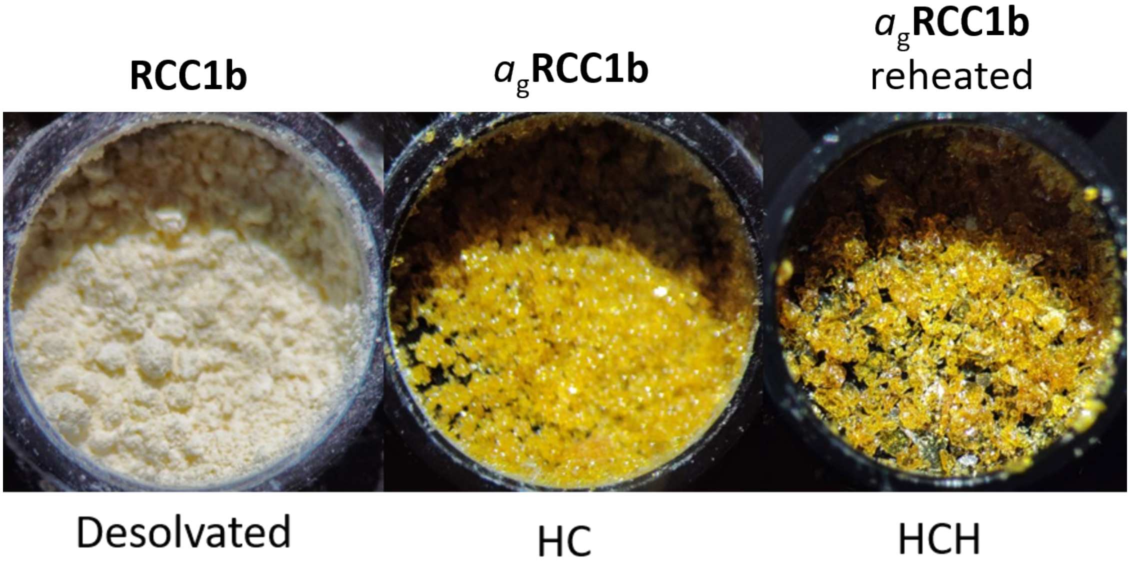

Supplementary Figure 33: Optical images of desolvated **RCC1b** sample prior to heating (left), a_g**RCC1b** after a heat-cool (HC) cycle to 280 °C (middle), and reheated a_g**RCC1b** after a heat-cool-heat (HCH) cycle to 280 °C (right).

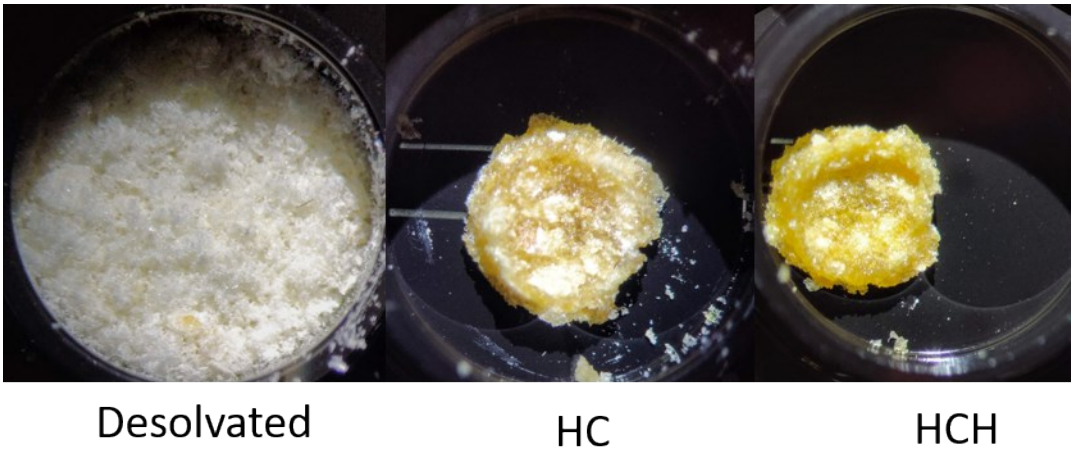

Supplementary Figure 34: Optical images of desolvated ***n*C_5-CC** (pentyl cage) sample prior to heating (left), after a heat-cool (HC) cycle to 170 °C (middle), and after a heat-cool-heat (HCH) cycle to 170 °C (right).

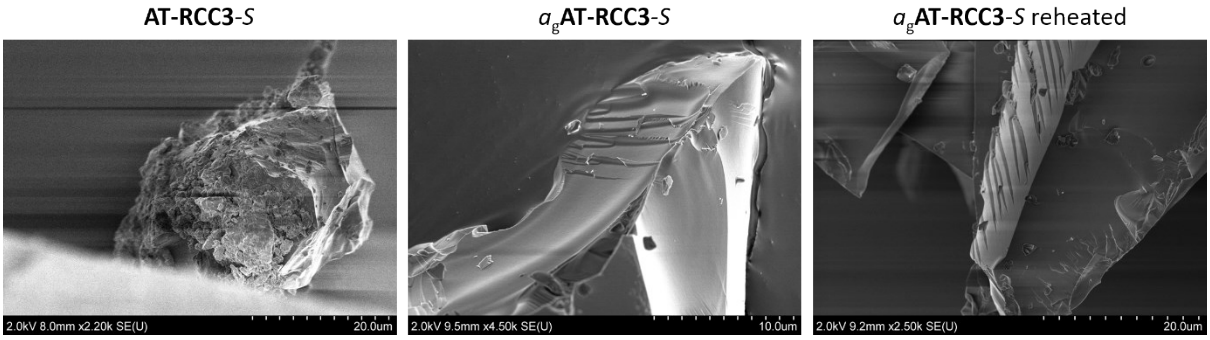
AT-RCC3-*S*
a_{g}**AT-RCC3**-*S*
a_{g}**AT-RCC3**-*S* reheated

Supplementary Figure 35: SEM images of desolvated **AT-RCC3**-*S* sample prior to heating (left), a_{g}**AT-RCC3**-*S* after a heat-cool (HC) cycle to 250 °C (middle), and reheated a_{g}**AT-RCC3**-*S* after a heat-cool-heat (HCH) cycle to 250 °C (right).

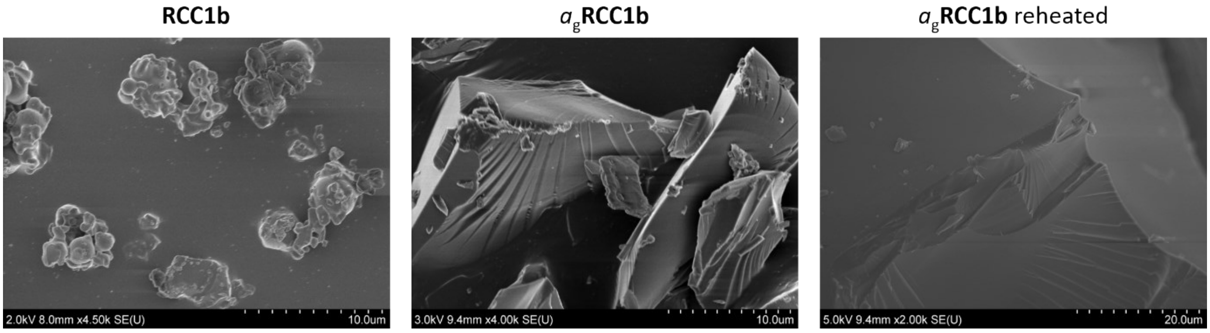
RCC1b
a_{g}**RCC1b**
a_{g}**RCC1b** reheated

Supplementary Figure 36: SEM images of desolvated **RCC1b** sample prior to heating (left), a_{g}**RCC1b** after a heat-cool (HC) cycle to 280 °C (middle), and reheated a_{g}**RCC1b** after a heat-cool-heat (HCH) cycle to 280 °C (right).

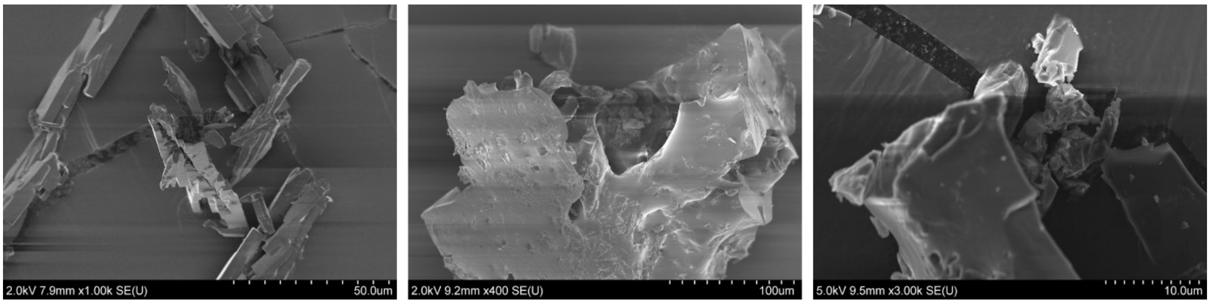

Supplementary Figure 37: SEM images of desolvated ***n*$\mathbf{C_5}$-CC** (pentyl cage) samples prior to heating (left), after a heat-cool (HC) cycle to 170 °C (middle), and after a heat-cool-heat (HCH) cycle to 170 °C (right).

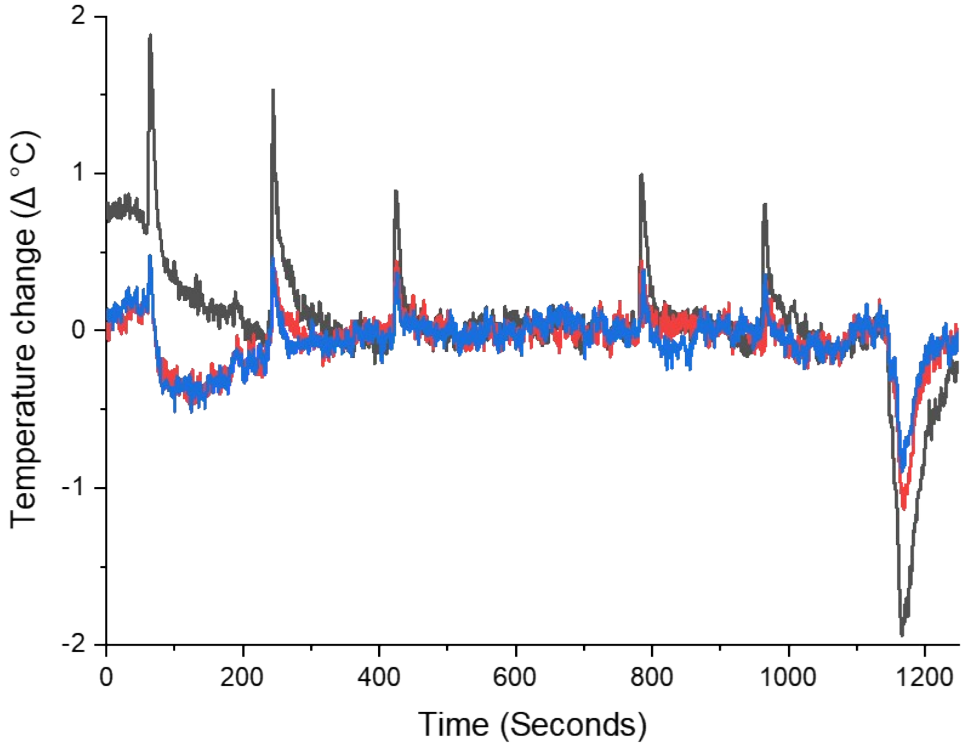

Supplementary Figure 38: High-throughput CO_2 uptake measurements on **RCC3**-*S* and a_g**RCC3**-*S*. As CO_2 is dosed into the evacuated samples of the cage and glass, an increase in temperature indicates the relative porosity of the samples – amorphous solids (black), melt-quenched glasses (red), and reheated glass samples above T_g (blue). The decrease in temperature after the gas additions occurs when the samples are re-evacuated.

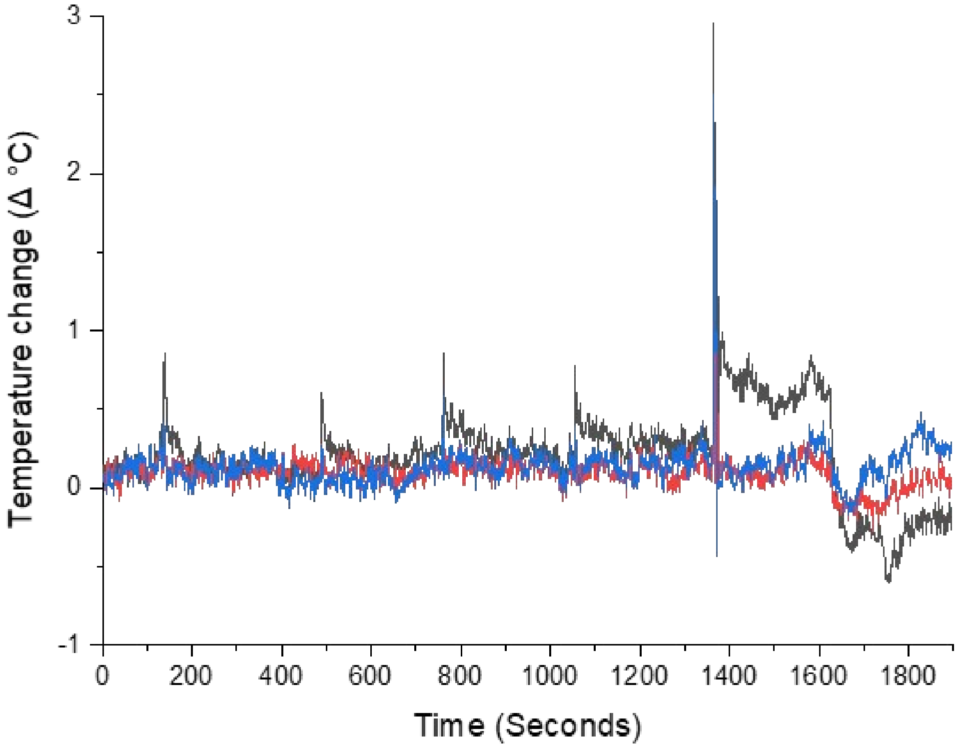

Supplementary Figure 39: High-throughput CO_2 uptake measurements on **AT-RCC3**-*S* and a_g**AT-RCC3**-*S*. As CO_2 is dosed into the evacuated samples of the cage and glass, an increase in temperature indicates the relative porosity of the samples – amorphous solids (black), melt-quenched glasses (red), and reheated glass samples above T_g (blue). The decrease in temperature after the gas additions occurs when the samples are re-evacuated.

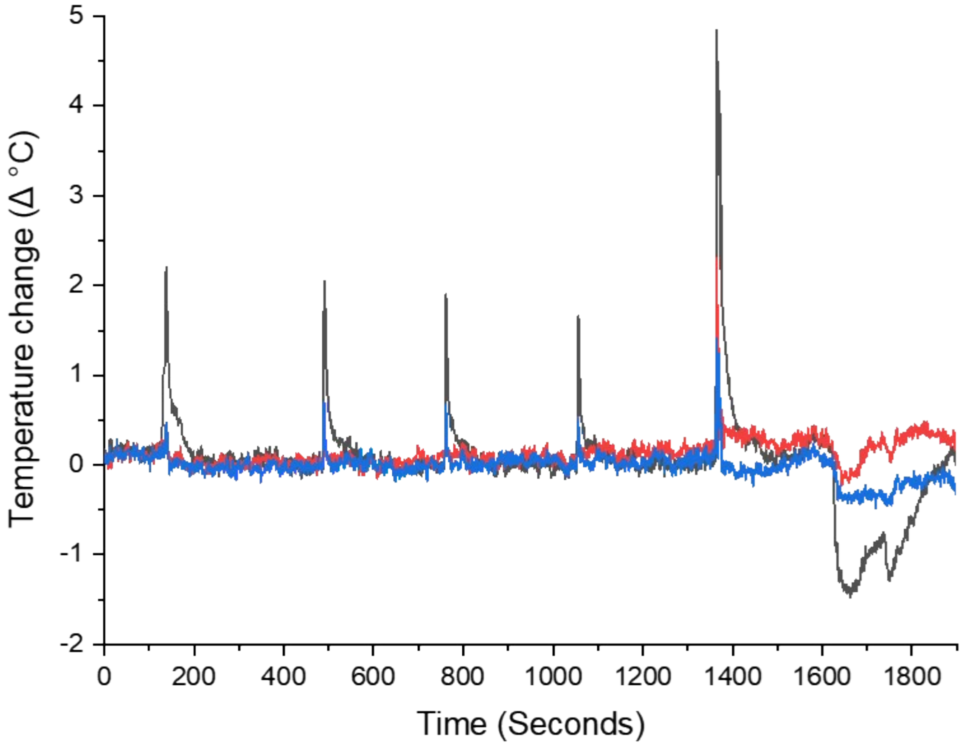

Supplementary Figure 40: High-throughput CO_2 uptake measurements on **RCC1b** and *a*$_g$**RCC1b**. As CO_2 is dosed into the evacuated samples of the cage and glass, an increase in temperature indicates the relative porosity of the samples – amorphous solids (black), melt-quenched glasses (red), and reheated glass samples above T_g (blue). The decrease in temperature after the gas additions occurs when the samples are re-evacuated.

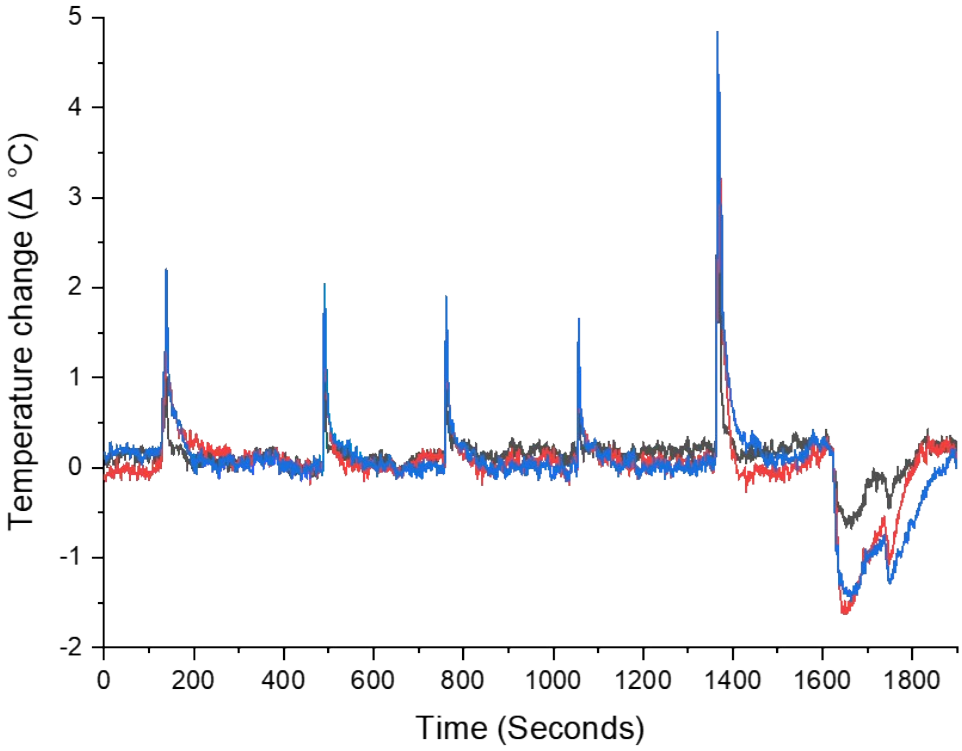

Supplementary Figure 41: High-throughput CO_2 uptake measurements on **RCC3**-*S* and a_{fg}**RCC3**-*S*. As CO_2 is dosed into the evacuated samples of the cage and glass, an increase in temperature indicates the relative porosity of the samples – amorphous solids (black), melt-quenched glasses (red), and reheated glass samples above T_g (blue). The decrease in temperature after the gas additions occurs when the samples are re-evacuated.

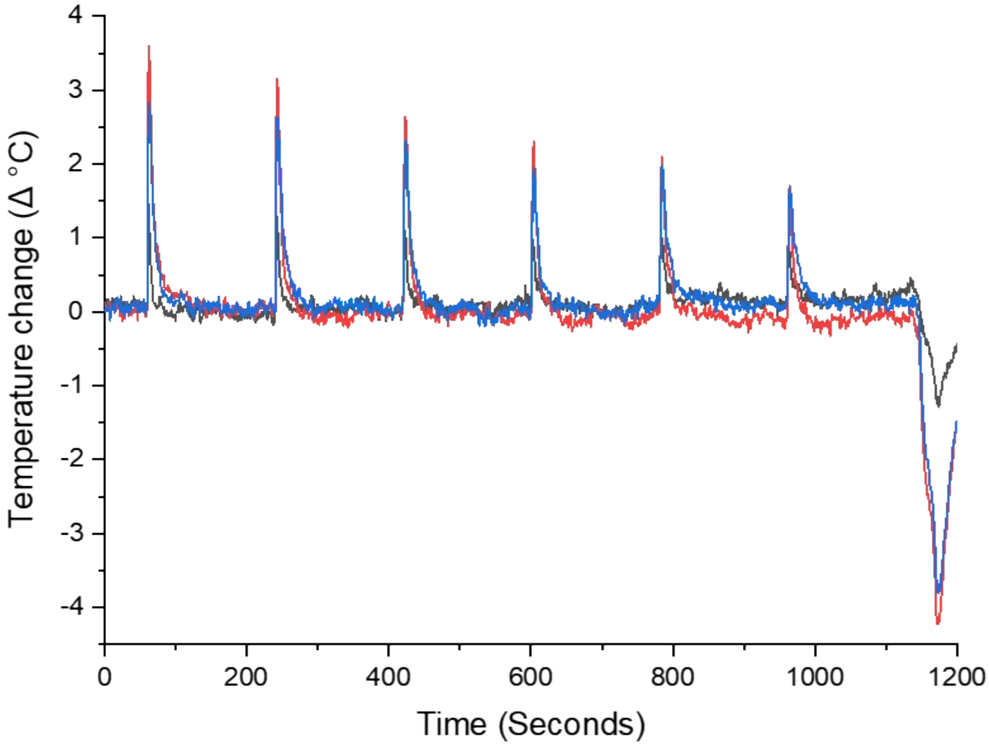

Supplementary Figure 42: High-throughput CH_4 uptake measurements on **RCC3**-*S* and *α*$_{fg}$**RCC3**-*S*. As CO_2 is dosed into the evacuated samples of the cage and glass, an increase in temperature indicates the relative porosity of the samples – amorphous solids (black), melt-quenched glasses (red), and reheated glass samples above T_g (blue). The decrease in temperature after the gas additions occurs when the samples are re-evacuated.

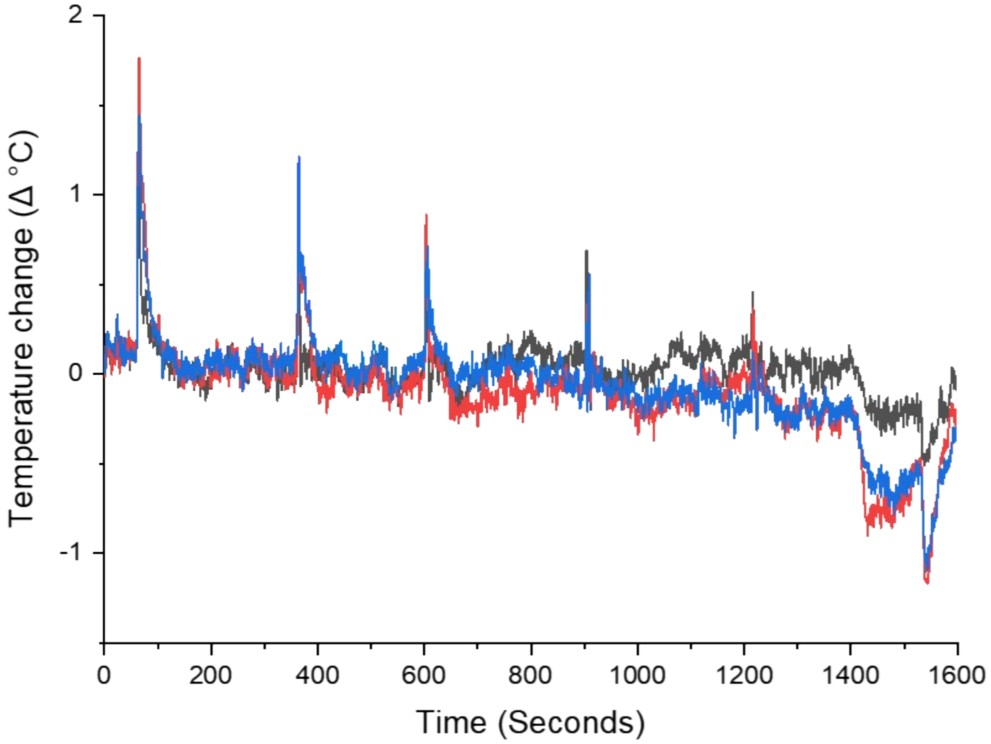

Supplementary Figure 43: High-throughput C_4H_{10} uptake measurements on **RCC3**-*S* and α_{fg}**RCC3**-*S*. As CO_2 is dosed into the evacuated samples of the cage and glass, an increase in temperature indicates the relative porosity of the samples – amorphous solids (black), melt-quenched glasses (red), and reheated glass samples above T_g (blue). The decrease in temperature after the gas additions occurs when the samples are re-evacuated.

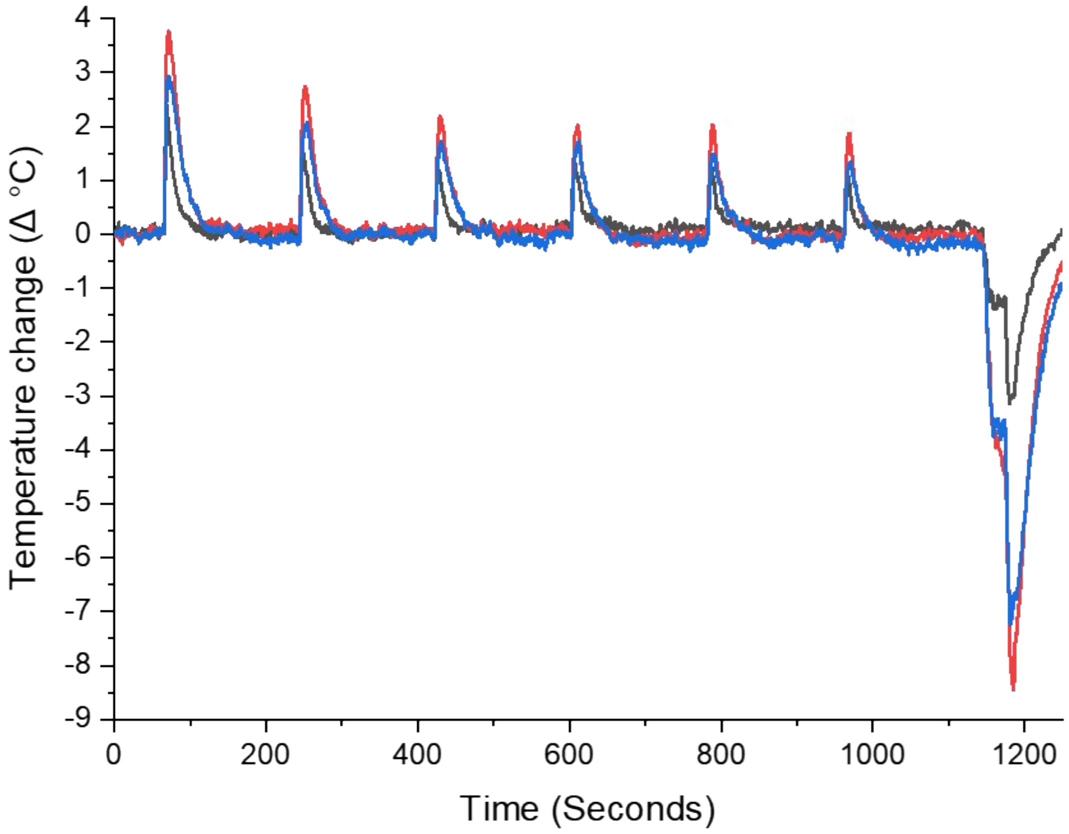

Supplementary Figure 44: High-throughput Xe uptake measurements on **RCC3**-*S* and a_{fg}**RCC3**-*S*. As CO_2 is dosed into the evacuated samples of the cage and glass, an increase in temperature indicates the relative porosity of the samples – amorphous solids (black), melt-quenched glasses (red), and reheated glass samples above T_g (blue). The decrease in temperature after the gas additions occurs when the samples are re-evacuated.

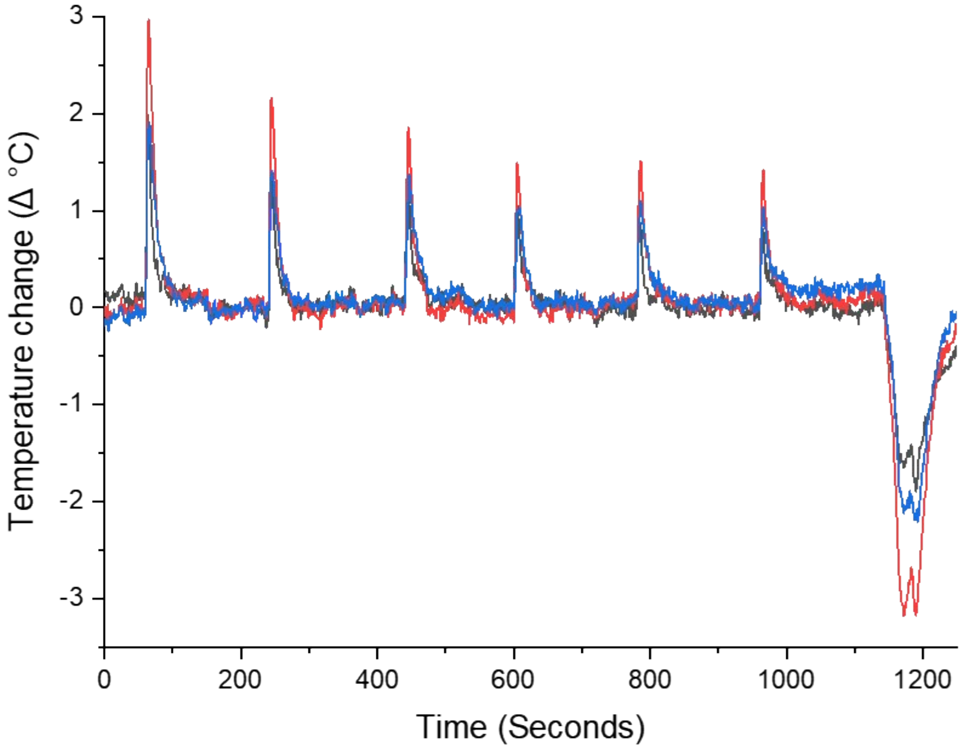

Supplementary Figure 45: High-throughput CO_2 uptake measurements on aged samples (6 weeks) of **RCC3**-*S* and *a*$_{\mathrm{fg}}$**RCC3**-*S*. As CO_2 is dosed into the evacuated samples of the cage and glass, an increase in temperature indicates the relative porosity of the samples – amorphous solids (black), melt-quenched glasses (red), and reheated glass samples above T_g (blue). The decrease in temperature after the gas additions occurs when the samples are re-evacuated.

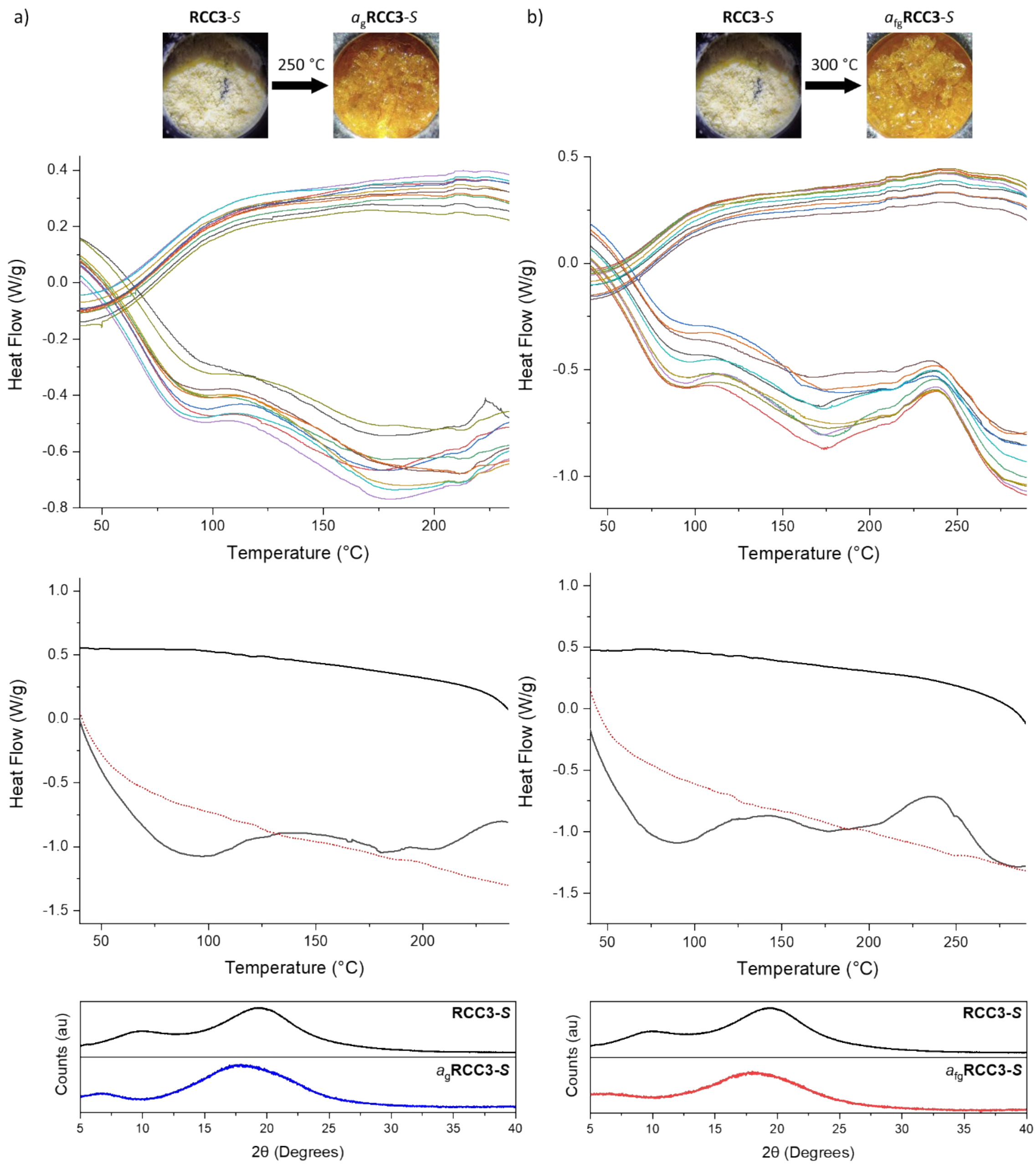

Supplementary Figure 46: Optical images, DSC traces of **RCC3**-*S* after being subjected to a heat-cool cycle and a heat-cool-heat cycle, and PXRD patterns at a) 250 °C (a_g**RCC3**-*S*) and b) 300 °C (a_{fg}**RCC3**-*S*). There are slight variations between the scale up and original DSC traces, in particular, the second endotherm of a_{fg}**RCC3**-*S* shows a wider endotherm in the scale up, rather than the sharp peak that is seen in the original DSC trace. Variations are likely due to the scale-up being performed on a different instrument with different pans - see **Supplementary Methods**.

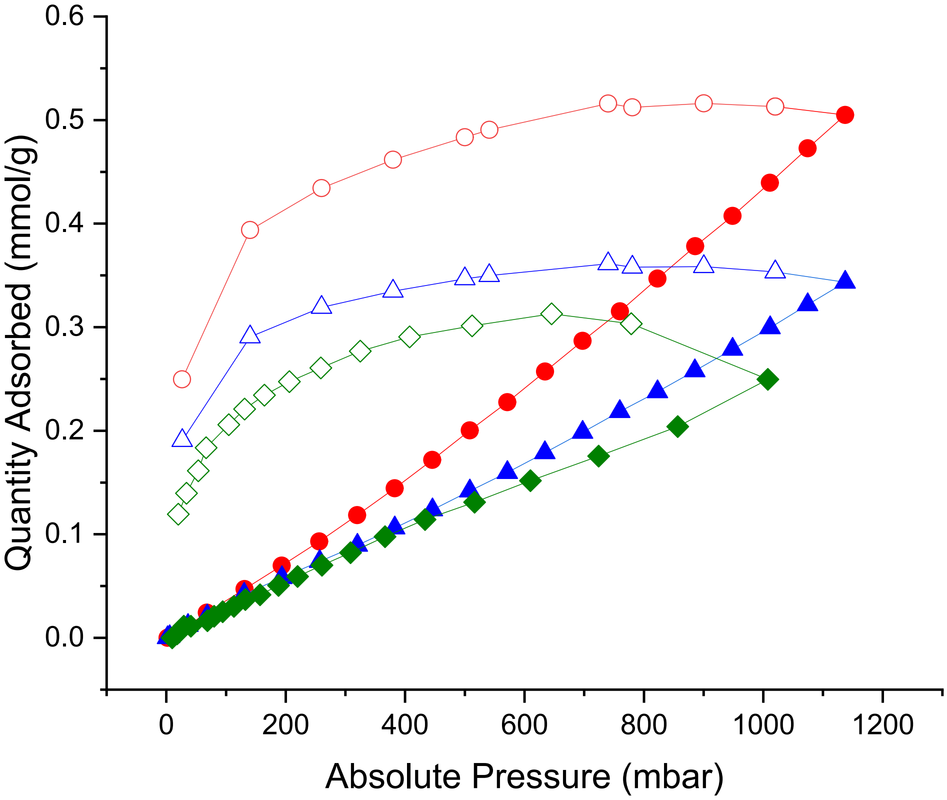

Supplementary Figure 47: CO_2 adsorption (filled) and desorption (empty) isotherms of **RCC3**-*S* and glass samples performed at 273 K. Red - a_g**RCC3**-*S* (prepared at 250 °C), blue - a_{fg}**RCC3**-*S* (prepared at 300 °C), and green - **RCC3**-*S* (as prepared).

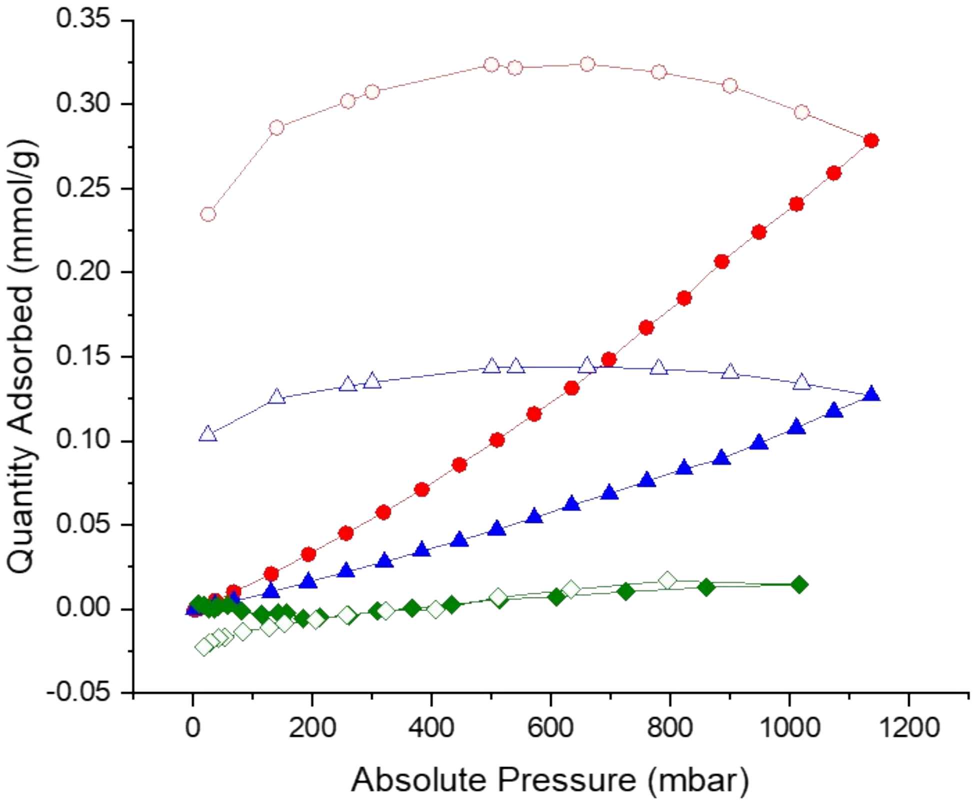

Supplementary Figure 48: CH_4 adsorption (filled) and desorption (empty) isotherms of **RCC3**-*S* and glass samples performed at 273 K. Red - a_g**RCC3**-*S* (prepared at 250 °C), blue - a_{fg}**RCC3**-*S* (prepared at 300 °C), and green - **RCC3**-*S* (as prepared).

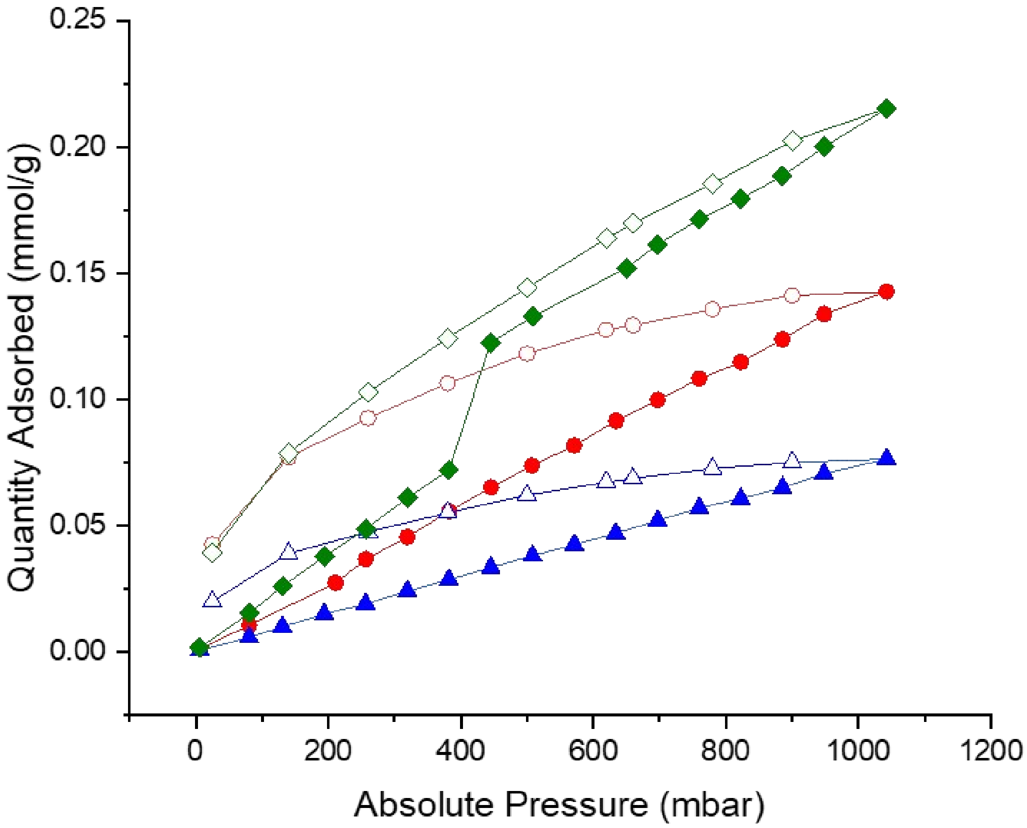

Supplementary Figure 49: Xe adsorption (filled) and desorption (empty) isotherms of **RCC3**-*S* and glass samples performed at 273 K. Red - a_g**RCC3**-*S* (prepared at 250 °C), blue - a_{fg}**RCC3**-*S* (prepared at 300 °C), and green - **RCC3**-*S* (as prepared).

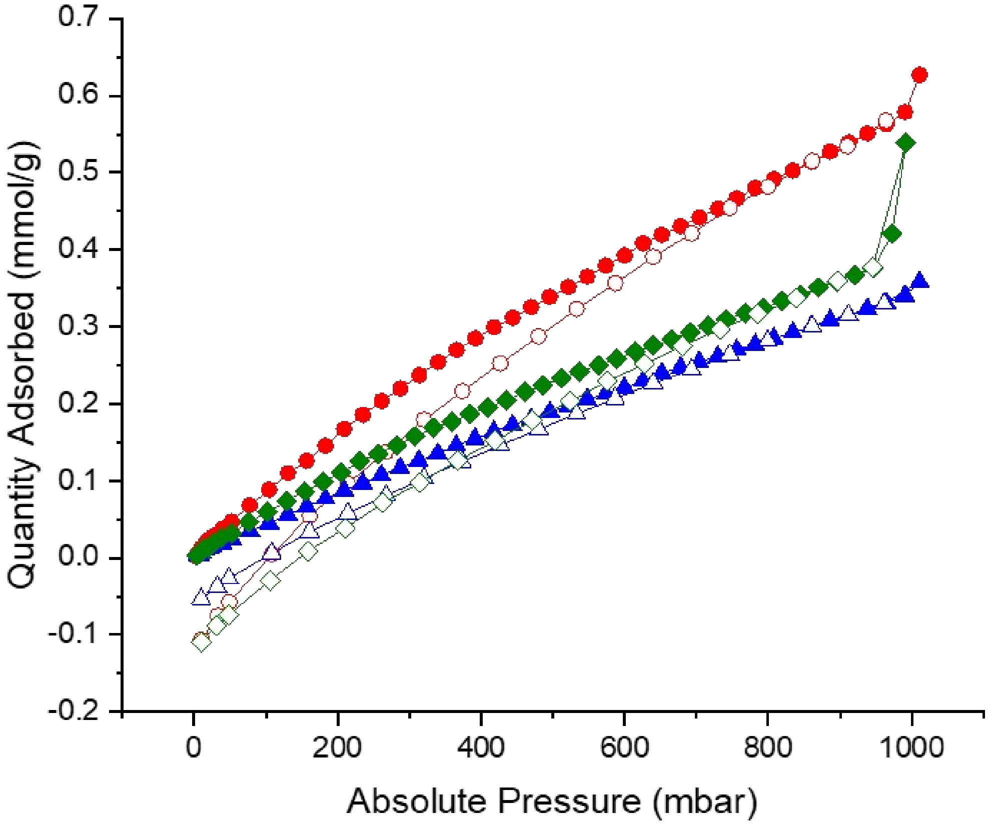

Supplementary Figure 50: N_2 adsorption (filled) and desorption (empty) isotherms of **RCC3**-*S* and glass samples performed at 77 K. Red - a_g**RCC3**-*S* (prepared at 250 °C), blue - a_{fg}**RCC3**-*S* (prepared at 300 °C), and green - **RCC3**-*S* (as prepared).

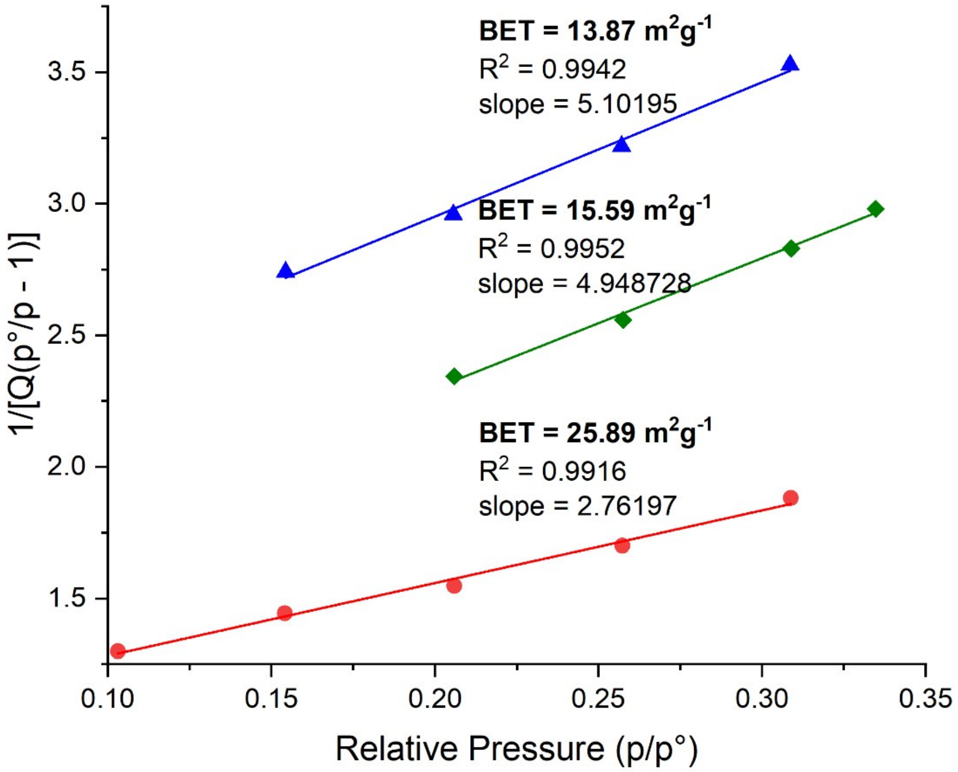

Supplementary Figure 51: BET plots of *a*$_{g}$**RCC3**-*S* (red), *a*$_{fg}$**RCC3**-*S* (blue), and **RCC3**-*S* (green). The BET surface area was calculated using a microporous assumption.

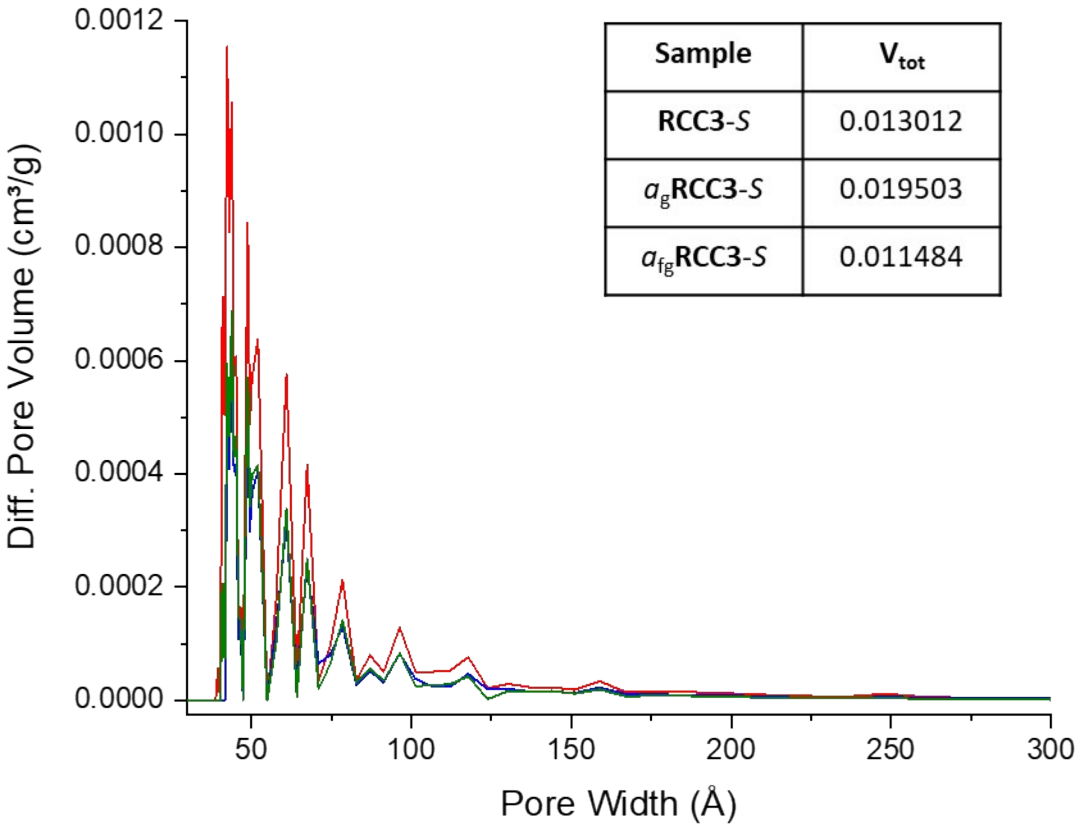

Sample	V_{tot}
RCC3-*S*	0.013012
a_g**RCC3**-*S*	0.019503
a_{fg}**RCC3**-*S*	0.011484

Supplementary Figure 52: Pore size distribution curves and pore volumes calculated at 0.95 bar obtained from the N_2 adsorption branch of the isotherm at 77 K of **RCC3**-*S* and glass samples using non-negative regularization model. Red - a_g**RCC3**-*S* (prepared at 250 °C), blue - a_{fg}**RCC3**-*S* (prepared at 300 °C), and green - **RCC3**-*S* (as prepared).

Supplementary Methods

General Synthetic and Analytical Methods

Materials: 1,3,5-Triformylbenzene (TFB) and (1*S*,2*S*)-cyclohexane-1,2-diamine (*S,S*-CHDA) were purchased from Manchester Organics; trifluoroacetic acid (TFA) was purchased from TCI UK; sodium borohydride, sodium sulfate, and ethylenediamine (EDA), triethylamine, napthoyl chloride, and formic acid were purchased from Sigma-Aldrich. Dichloromethane (DCM), methanol, chloroform, acetone, and hexane were reagent or HPLC grade and purchased from Fisher Scientific. (6*S*,7*S*)-Dodecane-6,7-diamine[3] was synthesised using (1*R*,2*R*)-1,2-bis(2-hydroxyphenyl)ethylenediamine and hexanal from Sigma-Aldrich, and toluene, 37% hydrochloric acid, and tetrahydrofuran (THF) from Fisher Scientific. All gases (nitrogen, carbon dioxide, methane, xenon, butane) were purchased from BOC at a purity of ≥ 99.9%. All chemicals and solvents were used as received without any purification.

Synthesis: All reactions were stirred magnetically using Teflon-coated stirring bars. Where heating was required, the reactions were warmed using a stirrer hotplate with heating blocks with the stated temperature being measured externally to the reaction flask with an attached probe. Removal of solvents was done using a rotary evaporator.

NMR Spectra: ^{1}H Nuclear magnetic resonance (NMR) spectra were recorded using an internal deuterium lock for the residual protons in $CDCl_3$ (δ = 7.26 ppm) at ambient probe temperature on a Bruker Avance 400 (400 MHz) instrument. NMR data are presented as follows: chemical shift, integration, peak multiplicity (s = singlet, d = doublet, t = triplet, q = quartet, m = multiplet, br = broad, app = apparent) and coupling constants (*J* / Hz). Chemical shifts are expressed in ppm on a δ scale relative to δ_{CDCl3} (7.26 ppm) and coupling constants, *J*, are given in Hz.

HRMS: High resolution mass spectrometry (HRMS) was carried out using an Agilent Technologies 6530B accurate-mass QTOF Dual ESI mass spectrometer (MeOH + 0.1% formic acid, 0.25 mL/min, capillary voltage 4000 V, fragmentor 225 V) in positive-ion detection mode.

Elemental Analysis: Elemental analysis of CHN was performed by the University of Liverpool's Department of Chemistry analytical services.

MPt: Obtained using Stuart SMP10 digital melting point apparatus and are reported uncorrected.

Optical DSC and Imaging Station: The broad melting behaviour of **RCC3**-*S* was recorded using a Linkam Scientific Optical DSC450 and imaging station.

TGA: Thermogravimetric analysis was carried out using a PerkinElmer TGA 8000 with an automated vertical overhead thermobalance. The sample was heated in ceramic sample pans under nitrogen at a rate of 10 °C/min to 600 °C.

DSC: Differential scanning calorimetry was performed on a TA instruments Discovery DSC. Heating and cooling rates were set at 10 °C/min up to the desired temperature. Samples were equilibrated at 20 °C before heating. Once the set upper temperature had been reached, samples were held at that temperature for 5 minutes before cooling. Measurements were performed under a flow of nitrogen set at 50 mL/min. Samples were prepared in air in Tzero aluminium hermetic pans and sealed with Tzero hermetic lid with pin hole (blue set).

For scale up of **RCC3**-*S* for gas sorption, a TA instruments Q2000 was used. Heating and cooling rates were set at 10 °C/min up to the desired temperature. Samples were equilibrated at 20 °C before heating. Once the set upper temperature had been reached, samples were held at that temperature for 5 minutes before cooling. Measurements were performed under a flow of nitrogen set at 50 mL/min. Samples were prepared in air in Tzero aluminium pans with Tzero lid (black set).

PXRD: Laboratory powder X-ray diffraction data were collected in transmission mode on samples held on a black opaque 96-shallow well microplate (ProxiPlate-96 Black) on a Panalytical X'Pert PRO MPD equipped with a high-throughput screening (HTS) XYZ stage, X-ray focusing mirror and PIXcel detector, using Ni-filtered Cu Kα radiation. Data were measured over the range 4–40° in ~0.013° steps over 60 minutes.

Raman: Raman spectroscopy was performed on a Reinshaw InVia™ Qontor® microscope. Samples were mounted on a metal slide. Samples were irradiated with two different wavelengths, 532 nm and 785 nm.

Optical Microscopy: Optical images were taken using a camera on an Olympus BX53 microscope.

SEM: Scanning electron microscopy (SEM) images were taken on a Hitachi S4800 SEM. Samples were prepared by depositing nanocrystals onto an adhesive high-purity carbon tab on 15mm Hitachi aluminium stubs, and coated in chromium before imaging.

High-Throughput Gas Sorption Analysis: High-throughput gas sorption was performed on a custom platform. A thermal camera is mounted above a sorption chamber and records the temperature change associated with gas adsorption/desorption. Samples were loaded into a 96-well ProxiPlate and degassed under vacuum whilst heating at 80 °C overnight and then left to equilibrate at 25 °C and maintained with a temperature-controlled oil heating unit. Whilst recording, the adsorbate gas is charged into the sorption chamber with approximately a 70 mbar dose. Samples were left to equilibrate for approximately 3 minutes before consecutive dosing. Data interpretation – 7 empty wells were averaged and used as a temperature change reference. This reference value was deducted from the measured temperature change in the sample wells giving temperature change in the samples.

Gas Sorption Analysis: Surface areas were measured by nitrogen sorption at 77 K. Samples were degassed offline at 90 °C for 15 h under dynamic vacuum (10^{-5} bar) before analysis, followed by degassing on the analysis port under vacuum. Isotherms were measured using a Micromeritics 2020 volumetric adsorption analyzer. Gas uptake measurements for CH_4, CO_2, and Xe were taken at a temperature of 273 K, stabilized using a circulating water chiller/heater, and N_2 were taken at a temperature of 77 K.

Synthesis and Characterisation of Organic Cages

CC3-*S*

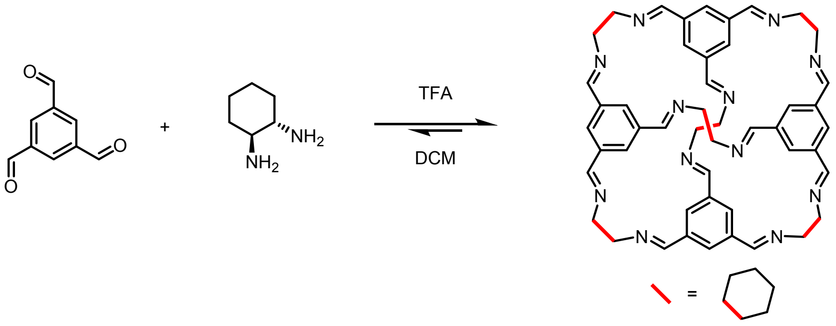

CC3-*S*

DCM (50 mL) was added onto 1,3,5-triformylbenzene (2.5 g, 15.41 mmol, 4.0 eq.), being careful so as not disturb the solid, followed by the addition of trifluoroacetic acid (50 µL). A solution of *(1S,2S)*-cyclohexane-1,2-diamine (*S,S*-CHDA, 2.64 g, 23.12 mmol, 6.0 eq.) in DCM (50 mL) was then carefully layered on top, and the reaction capped and left undisturbed for 5 days. The resulting crystals were collected by filtration, washed with methanol, and dried *in vacuo* to afford **CC3**-*S* as a colourless solid (2.96 g, 2.65 mmol, 68%).

^{1}H NMR (400 MHz, $CDCl_3$:d_4-MeOD) δ_H 8.02 (12H, s), 7.79 (12H, s), 3.28–3.21 (12H, m), 1.77–1.64 (12H, m), 1.56 (24H, br s), 1.41–1.27 (12H, m); **HRMS** (ES+) calc. for $C_{72}H_{84}N_{12}$ 1116.6936, found $[M+H]^{2+}$ 559.3411; **CHN** calc for $C_{72}H_{84}N_{12}$: C, 77.4; H, 7.6; N, 15.0%. Found C, 74.5; H, 7.5; N, 14.6%. Data in accordance with literature values.[1]

RCC3-*S*

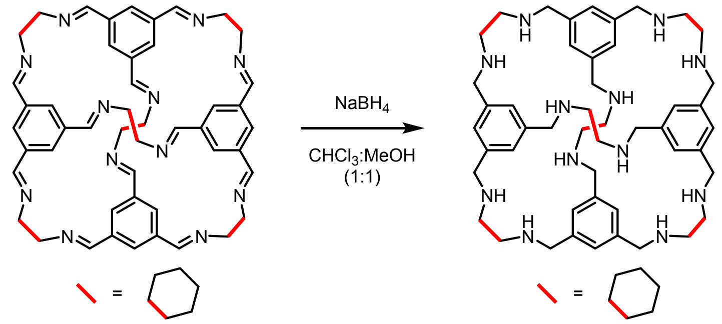

CC3-*S* **RCC3**-*S*

To a solution of **CC3**-*S* (5.0 g, 4.47 mmol, 1.0 eq.) in a mixture of CHCl$_3$:MeOH (1:1 v/v, 300 mL) was added NaBH$_4$ (5.42 g, 143.18 mmol, 32.0 eq.) under N$_2$. The resulting solution was stirred at room temperature overnight before the addition of water (10 mL). After stirring for a further 12 h, the solvent was removed *in vacuo*. The crude solid was partitioned between CHCl$_3$ and water, before the aqueous layer was extracted with CHCl$_3$ (3 x 50 mL). The combined organic layers were washed with water (3 x 100 mL), dried (Na$_2$SO$_4$), and concentrated *in vacuo* to afford a pale yellow foam which was ground into a solid (5.2 g, quant.).

^{1}H NMR (400 MHz, CDCl$_3$) δ_H 7.13 (12H, s), 3.82 (12H, d, *J* = 14.0 Hz), 3.57 (12H, d, *J* = 14.1 Hz), 2.20 (12H, d, *J* = 8.9 Hz), 2.00 (12H, d, *J* = 12.7 Hz), 1.65 (12H, d, *J* = 8.4 Hz), 1.20 – 1.12 (12H, m), 1.02 – 0.92 (12H, m).; **HRMS** (ES+) calc. for $C_{72}H_{108}N_{12}$ 1140.8814, found $[M+H]^+$ 1141.8632 and $[M+2H]^{2+}$ 571.4356; **CHN** calc for $C_{72}H_{108}N_{12}$: C, 75.7; H, 9.6; N, 14.7%. Found C, 71.4; H, 8.8; N, 13.9%. Data in accordance with literature values.[2]

AT-RCC3-*S*

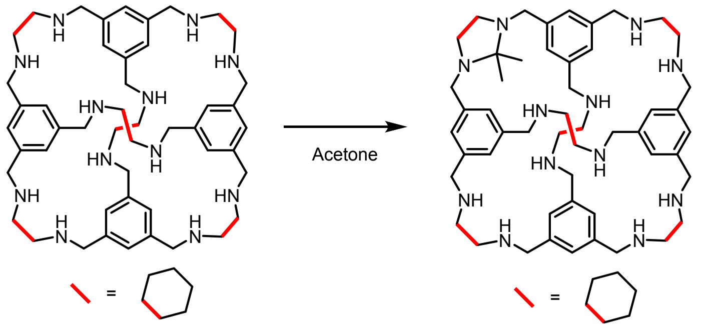

RCC3-*S* **AT-RCC3**-*S*

RCC3-*S* (2.65 g, 2.32 mmol, 1.0 eq.) was dissolved in acetone (160 mL) and left to stand overnight. The colourless crystals were collected by filtration and washed with acetone, before drying *in vacuo* to afford a colourless solid (1.48 g, 1.25 mmol, 53%).

^{1}H NMR (400 MHz, $CDCl_3$:d_4-MeOD) δ_H 7.22 – 6.71 (12H, m), 3.87 – 2.85 (24H, m), 2.34 – 0.61 (66H, m); **HRMS** (ES+) calc. for $C_{75}H_{112}N_{12}$ 1180.9127, found $[M+H]^+$ 1181.8979 and $[M+2H]^{2+}$ 591.4521; **CHN** calc for $C_{75}H_{112}N_{12}$: C, 76.2; H, 9.6; N, 14.2%. Found C, 74.5; H, 9.3; N, 14.1%. Data in accordance with literature values.[2]

***n*C$_5$-CC**

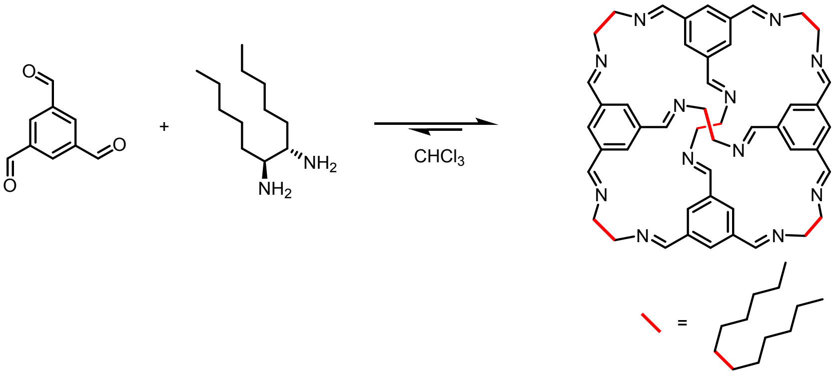

***n*C$_5$-CC**

A solution of 1,3,5-triformylbenzene (1.36 g, 8.42 mmol, 4.0 eq.) and (6S,7S)-dodecane-6,7-diamine (3.04 g, 15.17 mmol, 7.2 eq., synthesised according to previous literature methods[3]) in CHCl$_3$ (43 mL) was refluxed for 6 days before being allowed to cool to room temperature. The crude reaction was concentrated *in vacuo* before acetone was added to precipitate a pale brown solid which was collected by filtration. The solid was subsequently re-dissolved in a mixture of DCM/MeOH (1:1, 100 mL), insoluble precipitates were removed by filtration, and the DCM was carefully removed *in vacuo* until an off-white solid precipitated. The resulting solid was collected by filtration and dried further *in vacuo* to afford ***n*C$_5$-CC** as an off-white solid (55 mg, 0.034 mmol, 2%).

^{1}H NMR (400 MHz, CDCl$_3$) δ_H 8.05 (12H, s), 7.87 (12H, s), 3.33 (12H, dd, *J* = 5.8, 2.6 Hz4), 1.84 – 1.70 (12H, m), 1.69 – 1.58 (12H, m), 1.33 – 1.01 (72H, m), 0.84 (36H, t, *J* = 6.9 Hz); **HRMS** (ES+) calc. for $C_{108}H_{168}N_{12}$ 1634.3541, found $[M+H]^{2+}$ 818.1655; **CHN** calc for $C_{108}H_{168}N_{12}$: C, 79.4; H, 10.4; N, 10.3%. Found C, 78.3; H, 10.2; N, 10.0%. Data in accordance with literature values.[3]

RCC1b

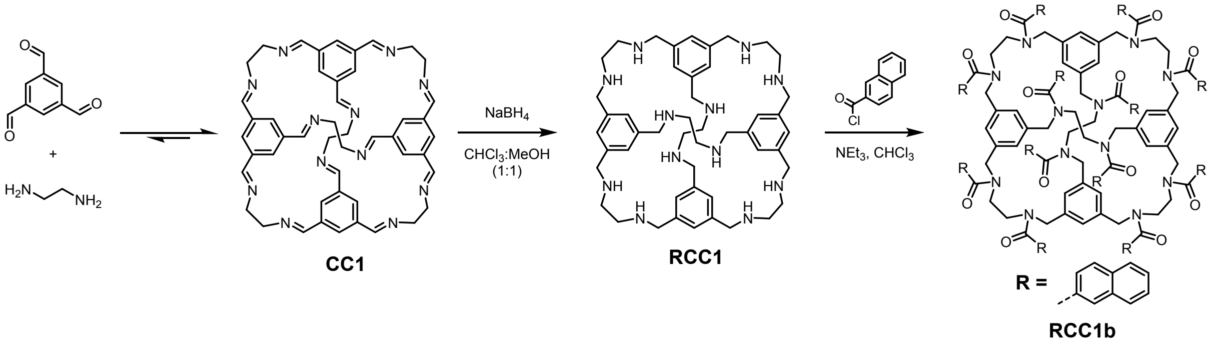

A solution of 1,3,5-triformylbenzene (3.0 g, 18.5 mmol, 4.0 eq.) was dissolved in DCM (920 mL) and transferred into a 5 L jacketed reactor. A solution of ethylenediamine (1.9 mL, 28.4 mmol, 6.1 eq.) dissolved in DCM (680 mL) was then added dropwise to the TFB solution at 0 °C over 48 hours, with overhead mechanical stirring. The resulting reaction mixture was filtered to remove any insoluble precipitate, and carefully concentrated *in vacuo* (water bath maintained below 20 °C), but not to dryness. Hexane was added to the concentrated solution to precipitate **CC1** which was collected by filtration to afford a **CC1** as a colourless solid (3.18 g, 4.01 mmol, 87%), and used directly without further purification.

CC1 (1.6 g, 2.01 mmol, 1.0 eq.) was dissolved in a mixture of $CHCl_3$/MeOH (1:1, 120 mL) by stirring, before $NaBH_4$ (2.44 g, 64.56 mmol, 32.0 eq.) was added batchwise under N_2. After complete addition, the reaction was stirred at room temperature for 18 h before the addition of water (5 mL). The mixture was stirred for a further 18 h before being concentrated *in vacuo*, and the resulting solid sonicated in $CHCl_3$. The filtrate was collected and concentrated *in vacuo* to afford **RCC1** as a colourless foamed solid (1.65 g, quant.) which was used directly to form **RCC1b**.

Triethylamine (2.56 mL, 18.36 mmol, 15.0 eq.) was added to a solution of **RCC1** (1.0 g, 1.22 mmol, 1.0 eq.) in anhydrous $CHCl_3$ (100 mL) under N_2 at 0 °C. After 15 min, a solution of napthoyl chloride (2.94 g, 15.42 mmol, 12.6 eq.) in anhydrous $CHCl_3$ (50 mL) was added dropwise. The resulting mixture was allowed to warm to room temperature and stirred for 6 days before being concentrated *in vacuo*. To the crude material was added THF (100 mL) and the slurry sonicated, before the colourless triethylamine hydrochloride salts were removed by filtration. The resulting orange filtrate was concentrated *in vacuo*, before the solid was stirred in MeOH (40 mL). The filtrate was decanted off of the solid, and the washing repeated a further 4 times, before the solid was collected by filtration and dried *in vacuo* to afford **RCC1b** as a pale yellow solid (1.39 g, 0.52 mmol, 42%).

^{1}H NMR (400 MHz $CDCl_3$) δ_H 8.06 – 7.15 (96H, m), 4.91 (24H, br s), 3.63 (24H, br s); **HRMS** (ES+) calc. for $C_{180}H_{144}N_{12}O_{12}$ 2666.1060, found $[M+2Na]^{2+}$ 1356.0058; **CHN** calc for $C_{180}H_{144}N_{12}O_{12}$: C, 81.1; H, 5.4; N, 6.3%. Found C, 78.3; H, 5.4; N, 6.5%. Data in accordance with literature values.[4]

Activation of Samples: All of the cages were desolvated in a vacuum oven at 90 °C (with the exception of **RCC3**-*S* which was desolvated at 130 °C) until analysis by TGA indicated no significant mass loss.

Scale-up method for RCC3-*S* glasses: Scaled-out batchwise by heating and cooling 10 samples of ~10 mg **RCC3**-*S* in separate aluminium DSC pans at 10 °C/min to either 250 °C (a_g**RCC3**-*S*) or 300 °C (a_fg**RCC3**-*S*). Samples were then removed from the aluminium pans and combined to recover a_g**RCC3**-*S* (42 mg) and a_fg**RCC3**-*S* (84 mg) which were analysed by PXRD and gas sorption.

Supplementary Video

Supplementary Video 1: Melting behaviour of **RCC3**-*S* between 80 and 200 °C at a heating rate of 10 °C/min using a Linkam Optical DSC450.

Supplementary References

1 T. Hasell, S. Y. Chong, K. E. Jelfs, D. J. Adams and A. I. Cooper, *J. Am. Chem. Soc.*, 2012, **134**, 588–598.

2 M. Liu, M. A. Little, K. E. Jelfs, J. T. A. Jones, M. Schmidtmann, S. Y. Chong, T. Hasell and A. I. Cooper, *J. Am. Chem. Soc.*, 2014, **136**, 7583–7586.

3 N. Giri, C. E. Davidson, G. Melaugh, M. G. Del Pópolo, J. T. A. Jones, T. Hasell, A. I. Cooper, P. N. Horton, M. B. Hursthouse and S. L. James, *Chem. Sci.*, 2012, **3**, 2153–2157.

4 J. L. Culshaw, G. Cheng, M. Schmidtmann, T. Hasell, M. Liu, D. J. Adams and A. I. Cooper, *J. Am. Chem. Soc.*, 2013, **135**, 10007–10010.